Diet-induced adipose tissue expansion is mitigated in mice with a targeted inactivation of mesoderm specific transcript (*Mest*)

Rea P. Anunciado-Koza[1], Justin Manuel[1], Randall L. Mynatt[2], Jingying Zhang[2], Leslie P. Kozak[3], Robert A. Koza[1]*

1 Center for Molecular Medicine, Maine Medical Center Research Institute, Scarborough, Maine, United States of America, **2** Transgenics Core Facility, Pennington Biomedical Research Center, LSU System, Baton Rouge, Louisiana, United States of America, **3** Institute of Animal Reproduction and Food Research, Polish Academy of Sciences, Olsztyn, Poland

* rkoza@mmc.org

Abstract

Interindividual variation of white adipose tissue (WAT) expression of mesoderm specific transcript (*Mest*), a paternally-expressed imprinted gene belonging to the α/β-hydrolase fold protein family, becomes apparent among genetically inbred mice fed high fat diet (HFD) and is positively associated with adipose tissue expansion (ATE). To elucidate a role for MEST in ATE, mice were developed with global and adipose tissue inactivation of *Mest*. Mice with homozygous (*Mest*^gKO) and paternal allelic (*Mest*^pKO) inactivation of *Mest* were born at expected Mendelian frequencies, showed no behavioral or physical abnormalities, and did not perturb expression of the *Mest* locus-derived microRNA miR-335. *Mest*^pKO mice fed HFD showed reduced ATE and adipocyte hypertrophy, improved glucose tolerance, and reduced WAT expression of genes associated with hypoxia and inflammation compared to littermate controls. Remarkably, caloric intake and energy expenditure were unchanged between genotypes. Mice with adipose tissue inactivation of *Mest* were phenotypically similar to *Mest*^pKO, supporting a role for WAT MEST in ATE. Global profiling of WAT gene expression of HFD-fed control and *Mest*^pKO mice detected few differences between genotypes; nevertheless, genes with reduced expression in *Mest*^pKO mice were associated with immune processes and consistent with improved glucose homeostasis. Ear-derived mesenchymal stem cells (EMSC) from *Mest*^gKO mice showed no differences in adipogenic differentiation compared to control cells unless challenged by shRNA knockdown of *Gpat4*, an enzyme that mediates lipid accumulation in adipocytes. Reduced adipogenic capacity of EMSC from *Mest*^gKO after *Gpat4* knockdown suggests that MEST facilitates lipid accumulation in adipocytes. Our data suggests that reduced diet-induced ATE in MEST-deficient mice diminishes hypoxia and inflammation in WAT leading to improved glucose tolerance and insulin sensitivity. Since inactivation of *Mest* in mice has minimal additional effects aside from reduction of ATE, an intervention that mitigates MEST function in adipocytes is a plausible strategy to obviate obesity and type-2-diabetes.

Introduction

The global rise in obesity rates are caused by interactions between an individual's genetic predisposition, the environment and epigenetic factors. The genetic component has been clearly demonstrated in studies of monozygotic twins with heredity predicted to account for ~40–70% of obesity [1, 2]. However, recent genome wide association studies (GWAS) of 97 body mass index (BMI)-associated loci in >300K individuals was shown to account for only <3% of the variance of BMI [3]. Although it is estimated that risk alleles may account for up to ~20% of this variance [3], a large percentage of BMI is unexplained which underscores the complexity of interactions between genomic, environmental and epigenetic components [4–6]. Therefore, the use of murine models in which the genetic background and environment can be carefully controlled is a powerful tool for the identification of potential epigenetic determinants associated with the development of obesity and related disease.

Variable development of diet-induced obesity (DIO) and type 2-diabetes (T2D) within inbred populations of mice has been well described [7–11] and shown to be stable among individual animals which suggests that an epigenetic mechanism is likely involved in its etiology [10, 12, 13]. Analyses of gene expression in white adipose tissue (WAT) of inbred C57BL/6J mice that showed diversity in DIO identified a novel set of genes that correlate with fat mass accretion [10, 13–16]. Mesoderm specific transcript (*Mest*), a maternally imprinted gene, showed variations of mRNA up to ~80-fold in WAT from individual mice fed an obesogenic diet which was positively associated with the rate of fat mass deposition [10, 16]. In addition, *Mest* mRNA in WAT biopsies prior to feeding mice an obesogenic diet was predictive of future inter-individual development of DIO [10]. Compelling evidence for a role for *Mest* in facilitating fat accumulation was obtained by transgenic overexpression of *Mest* in cell culture and in mouse adipose tissue; and, in the analyses of *Mest* gene and protein in WAT during developmental growth and in adult mice fed dietary fat [7, 10, 13, 14, 16–20]. Recent studies have determined that adipose tissue as well as blood levels of *Mest* mRNA is a rapid and early biological indicator of adipose tissue expansion (ATE) in mice [21]. ATE, or fat mass expansion, is a characteristic of obesity caused predominantly by triglyceride storage and expansion of adipocytes (i.e. adipocyte hypertrophy), and to a lesser extent, increased adipocyte hyperplasia [22, 23].

The positive association of *Mest* with ATE has been well established; however, little is known in regards to the catalytic function of MEST and whether its activity directly contributes to adipocyte hypertrophy and/or adipose tissue remodeling. MEST belongs to the α/β-hydrolase family of proteins [24, 25] and contains the catalytic triad serine-histidine-aspartate (amino acids 145–147) which is commonly associated with serine proteases, lipases and acyltransferases [24, 26]. Evidence showing that MEST is localized within the endoplasmic reticulum/Golgi apparatus of the adipocyte further supports its function in the facilitation of fat storage in adipocytes [16, 20, 27]. Alternatively, MEST contains a conserved epoxide-coordinating tyrosine in its sequence and shows sequence similarity to epoxide hydrolases from *M. tuberculosis* [28, 29]. Epoxide hydrolases modulate levels of epoxy fatty acids and their diol derivatives which have been shown to act as endogenous mediators of PPARs alpha and gamma [30–34]. Studies have shown that epoxyeicosatrienoic acid (EET) analog treatment suppresses adipogenesis of 3T3-L1 preadipocytes and reduces ATE and improves glucose tolerance in mice fed a high fat diet [35]. It has been suggested that mitigation of adipogenic differentiation by EET may occur via Pgc1α-dependent activation of the heme oxygenase-1 (*Hmox1*)-pAKT signaling pathway [36, 37]. Other studies suggest that *Mest* may act to attenuate Wnt signaling in 3T3-L1 cells by inhibiting the maturation and exit of LRP6 from the endoplasmic reticulum by controlling its glycosylated state [27].

In adult mice, MEST protein is highly expressed in white adipose tissue with very little or undetectable expression observed in brown adipose tissue, whole brain, liver, heart, kidney and spleen [16]. Recent studies suggest that human MEST could be an epigenetic target for periconceptual or intrauterine environmental exposures, such as parental obesity and gestational diabetes, leading to changes in its methylated state [38, 39]. Although few studies have examined MEST with respect to human adipose tissue, it has been shown that MEST is induced during adipogenesis of isolated human adipocytes [40, 41] and human abdominal subcutaneous white adipose tissue biopsies show increased MEST mRNA in obese compared to non-obese individuals [41].

In this study we generated isogenic mouse models with both global and conditional targeted inactivation of *Mest* to investigate its role in adipose tissue development and expansion. Our data suggests that MEST contributes to ATE by facilitating lipid accumulation in adipocytes in an obesogenic environment thereby enhancing hypoxia and inflammation which lead to impaired glucose tolerance and insulin sensitivity.

Results

Validation of gene targeted *Mest* knockout mice

A targeting vector containing a neomycin (NEO) selection cassette was used to insert loxP sites immediately 5' and 3' of *Mest* exon 3 using C57BL/6J (B6) ES cells (Fig 1A). Subsequent breeding of mice with germline transmission of the targeted *Mest* allele with *Ella*-cre transgenic mice resulted in the selection of progeny with deletions of only the NEO cassette or the floxed region (NEO cassette and *Mest* exon 3) resulting in an intact floxed or a global deletion of *Mest* exon 3. Deletion of exon 3 of *Mest* creates a stop codon in exon 4 and full inactivation of *Mest* as shown by the absence of *Mest* mRNA in white adipose tissue (WAT) of homozygous knockout (*Mest*$^{\mathbf{gKO}}$) mice (Fig 1B). *Mest*, an imprinted gene that is almost exclusively expressed from the paternal allele in adult mice [42–45] and highly expressed in WAT [10, 16, 46], is completely abrogated in mice with a paternal allelic inactivation of *Mest* (*Mest*$^{\mathbf{pKO}}$), but shows fully intact mRNA and protein levels when the maternal allele of *Mest* is selectively inactivated (*Mest*$^{\mathbf{mKO}}$; Fig 1B and 1C). Unlike previous observations showing abnormal maternal behavior and high incidence of postnatal mortality in mice with global or paternal inactivation of *Mest* on a mixed B6/129 background (Lefebvre et al 1998), our studies indicate normal litter sizes reared by dams with inactivated *Mest* (~8.2 pups/litter); and non-skewed gender (29 female/30 male) and genotype ratios with 14 wildtype (WT), 30 *Mest*$^{\mathbf{mKO}}$ or *Mest*$^{\mathbf{pKO}}$ and 15 *Mest*$^{\mathbf{gKO}}$ (chi-square 0.119; P = 0.998) born from crosses between heterozygous females and males. The basis for phenotypic differences in maternal behavior and early post-natal mortality between our studies and those of Lefebvre et al 1998 [43] are not known.

Since the *Mest* locus harbors a microRNA (miR-335), which has also been implicated in adipogenesis and lipid metabolism [47, 48], within an intronic sequence between exons 2 and 3 of *Mest* transcript variant 2 (TV2), an analyses was performed to determine whether the close proximity of a loxP site (Fig 1D) from the targeting vector aberrantly affects expression of miR-335. Analyses of inguinal (iWAT) WAT of 6–7 day old mice, a developmental time period when fat mass is rapidly expanding and WAT *Mest* is highly expressed [16], showed no differences in miR-335 expression in mice with intact (WT and *Mest*$^{\mathbf{mKO}}$) versus inactivated (*Mest*$^{\mathbf{gKO}}$ and *Mest*$^{\mathbf{pKO}}$) *Mest* (Fig 1E). In addition, RT-PCR analyses of 3 known transcriptional variants of *Mest* in mice that vary in the use of alternative exons (Fig 1D) shows that transcript variant 2 (TV2; NM_008590.2) is predominantly expressed in both subcutaneous iWAT and visceral epididymal (eWAT) WAT depots (Fig 1F). *Mest* TV1, which uses an additional alternative exon in the 5' coding region compared to TV2, also shows a low level of
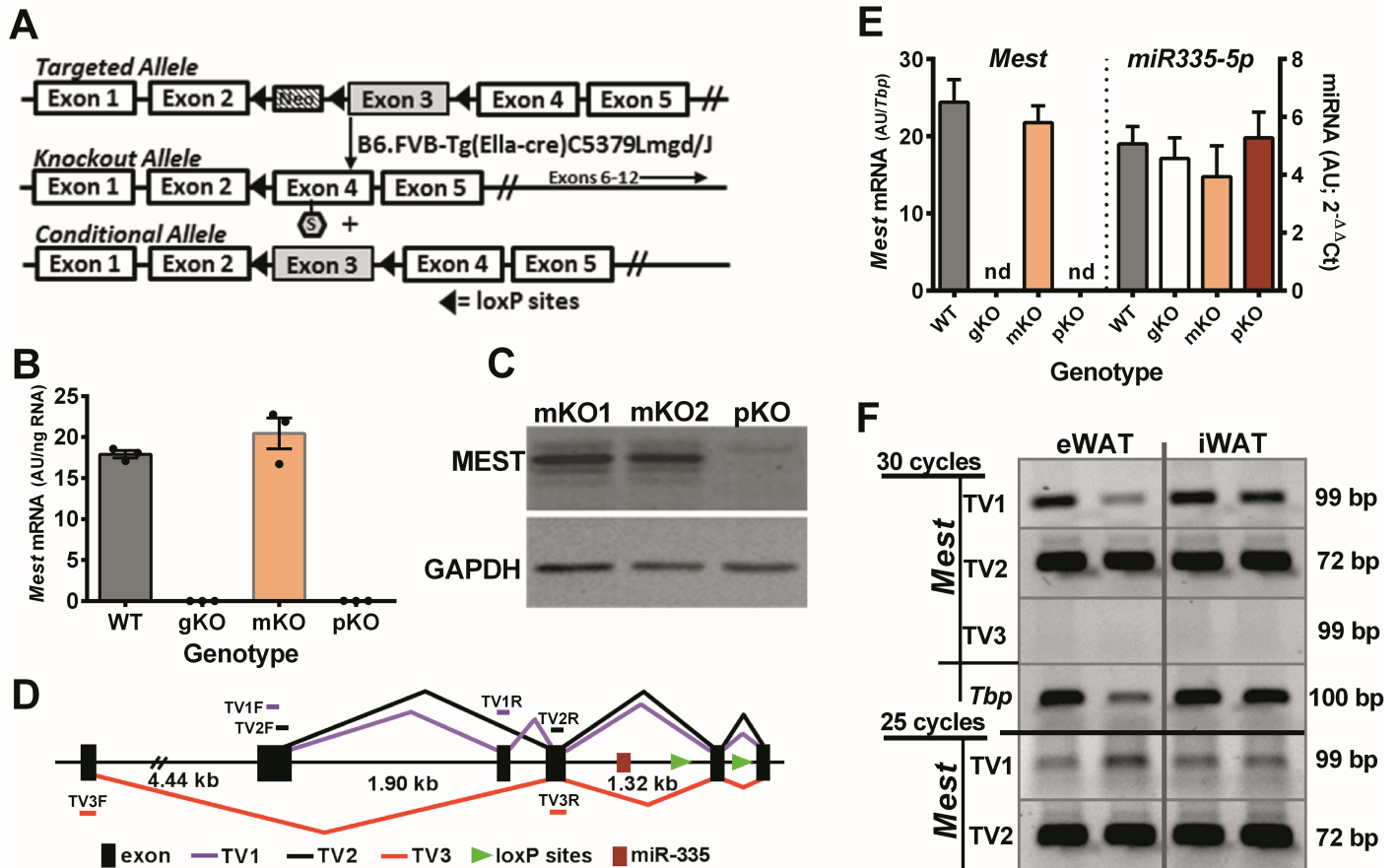
Fig 1. Validation of targeted *Mest* allele. (A) Representation of the targeted allele for mesoderm specific transcript (*Mest*) with *lox*P sites flanking *Mest* exon 3 and a Neo cassette located in intron 2. Deletion of *Mest* exon 3 causes a frameshift mutation and the generation of a stop codon (indicated with a hexagon containing an 'S') in *Mest* exon 4. (B) Analyses of *Mest* mRNA in adipose tissue of wildtype (WT; n = 3) mice and mice with homozygous (gKO; n = 3), maternal (mKO; n = 3) and paternal (pKO; n = 3) allelic inactivation of *Mest* by qRT-PCR showed complete loss of mRNA in adipose tissue of *Mest* gKO and pKO mice. (C) Western blot analysis shows MEST protein in adipose tissue of 2 mice with maternal allele inactivation of *Mest* (mKO1 and mKO2) whereas MEST protein is completely absent in adipose tissue of mice with a paternal allele inactivation of *Mest* (pKO). (D) Representation of the Mest gene showing location of *miR-335* near the proximal *lox*P site of the targeted *Mest* allele and 3 known splice variants (TV1, TV2 and TV3) for murine *Mest*. Small bars located above and below the diagram indicate the approximate location of forward reverse primers used to measure relative levels of each variant in adipose tissue. (E) QRT-PCR analyses of *Mest* and *miR-335* expression in total RNA isolated from 4–7 iWAT depots for each of 4 genotypes of 6–7 day old mice indicates that deletion of *Mest* exon 3 has minimal effect on *miR-335* expression. Levels of *Mest* and miR-335 expression are presented as the mean ± SEM. (F) RT-PCR analyses for 30 and 25 cycles indicates that transcript variant 2 (TV2; NM_008590.2) is the predominant *Mest* isoform in both epididymal white adipose tissue (eWAT) and inguinal white adipose tissue (iWAT). Sizes of PCR products for each of the transcript variants and TATA-box binding protein (*Tbp*) are shown on the right hand side of the figure.

expression in WAT, whereas TV3, a variant of *Mest* mRNA that uses an alternative 5'UTR ~4.5 kb upstream from the 5'UTR containing exon of TV1 and TV2, was absent in WAT (Fig 1F).

Bodyweight and body composition

Since *Mest*$^{\text{pKO}}$ mice do not express *Mest* mRNA or protein in WAT (Fig 1B and 1C), male progeny (WT and *Mest*$^{\text{pKO}}$) for the dietary obesity study were generated from a cross between female WT and male *Mest*$^{\text{mKO}}$ mice. From weaning (week 3) until 8 weeks of age, *Mest*$^{\text{pKO}}$ mice showed a small but significant reduction in body weight (Fig 2A) but no differences in adiposity measured as the ratio of fat mass/lean mass (Fig 2B) compared to WT littermate
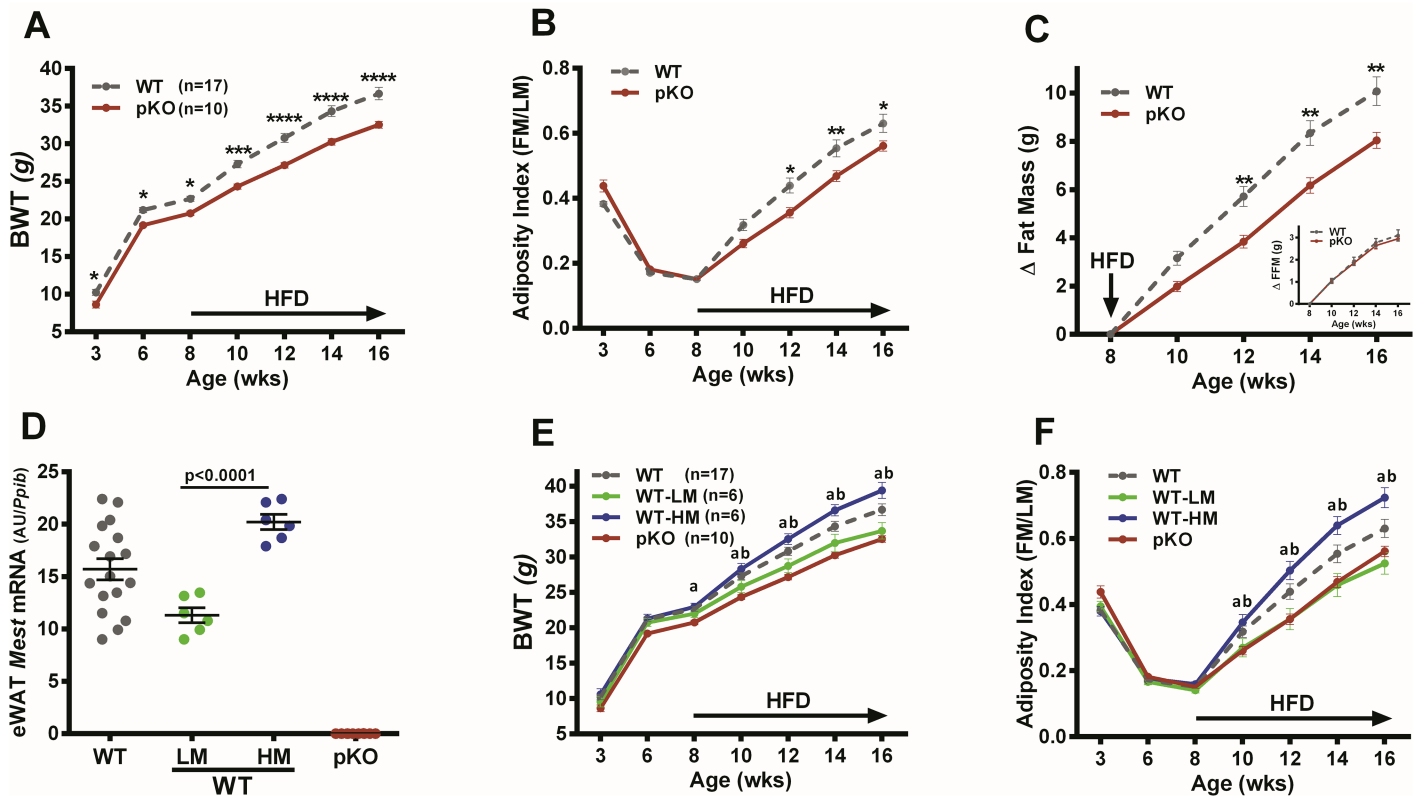
Fig 2. Dietary obesity in mice with inactivated *Mest*. (A) Longitudinal measurement of bodyweight (BWT) in 17 wildtype (WT) mice and 10 mice with inactivation of *Mest* on the paternal allele (pKO). Mice were fed high fat diet (HFD) from 8 to 16 weeks of age as indicated by the arrow along the X-axis. (B) Longitudinal measurements show the ratio of fat mass (FM) and lean mass (LM) measured by NMR, indicated as adiposity index (FM/LM), in 17 WT and 10 pKO mice fed a HFD from 8 to 16 weeks as shown by the arrow along the X-axis. (C) Data shows the cumulative change of fat mass (Δ Fat Mass) and fat-free mass (Δ FFM; inset graph) of 17 WT and 10 *Mest*^{pKO} (pKO) mice after initiation of a HFD at 8 weeks of age until 16 weeks of age as indicated on the X-axis. (D) Data represents tertiles of mice from the 17 WT mice in the study with the lowest (WT-LM; n = 6) and highest (WT-HM; n = 6) epididymal white adipose tissue (eWAT) *Mest* expression. Gene expression was measured by TaqMan QRT-PCR and is represented as arbitrary units (AU) normalized to cyclophilin b (*Ppib*). (E) Longitudinal analyses of BWT and (F) adiposity index in mice within WT-LM and WT-HM tertiles for eWAT *Mest* and pKO mice are shown. Data in all figures are presented as the mean ± SEM. Significance at each time point of the longitudinal phenotypic analyses between WT and pKO (A- C) was determined by 2-way ANOVA using the Holm-Sidak multiple comparisons test. Time points annotated with 1, 2, 3 or 4 asterisks indicate significant differences of P≤0.05, P≤0.01, P≤0.001 and P≤0.0001 respectively. Significance in eWAT *Mest* RNA expression between the WT-LM and WT-HM groups (D) was measured by a two-tailed unpaired parametric t-test and is indicated on the bar graph. Longitudinal data for WT-LM, WT-HM and pKO (E and F) was performed using 2-way ANOVA using Tukey's multiple comparisons test. Annotation with 'a' and 'b' indicates significant differences between WT-HM vs pKO and WT-HM vs WT-LM mice respectively.

controls. However, when fed an obesogenic diet (58 kcal% fat) from 8 until 16 weeks of age, dietary fat-induced increases in bodyweight, adiposity and fat mass deposition in *Mest*^{pKO} mice was significantly attenuated compared to WT mice (Fig 2A, 2B and 2C) whereas fat free mass (FFM) was unaffected (Fig 2C; inset). Regression analyses of the 17 WT mice at 16 weeks of age showed a strong correlation between eWAT *Mest* mRNA and fat mass deposition (R = 0.70; p<0.002) as well as *Mest* mRNA expression among adipose depots (iWAT vs eWAT *Mest*; R = 0.59; P<0.02) within each mouse which is consistent with previous studies [10, 16]. Analyses of subgroups of WT mice within the lowest (n = 6; WT-LM) and highest (n = 6; WT-HM) tertiles for eWAT *Mest* mRNA (Fig 2D) showed significant differences in BWT and adiposity between groups (Fig 2E and 2F). However, no differences were observed between WT-LM and *Mest*^{pKO} mice (Fig 2E and 2F). These data suggest that the low level of MEST in adipose tissue of WT-LM mice does not significantly contribute to additional ATE beyond

that observed for *Mest*^PKO mice. Thus, increased ATE only becomes apparent in mice that show high interindividual WAT *Mest* expression.

Adipose tissue inactivation of *Mest*

Mice with a floxed paternal allele for *Mest (Mest*^pFL; Fig 1A*)* were crossed with *Adipoq*-cre transgenic mice to generate animals with an *Adipoq*-cre mediated inactivation of the paternal allele (*Mest*^ApKO) of *Mest*. Analyses of WAT *Mes*t mRNA in cohorts of 5–17 age-matched male mice fed an obesogenic diet for 16 weeks showed a >98% reduction in both iWAT and eWAT *Mest* mRNA expression (Fig 3A) in *Mest*^ApKO mice compared with the 3 control groups (i.e. WT, WT-cre and *Mest*^pFL; Fig 3A) and supports previous studies showing that *Mest* is expressed in the mature adipocyte fraction of adipocytes [10, 20]. In addition, the presence of *loxP* sites in the 5' and 3' introns surrounding *Mest* exon 3 of *Mest*^pFL did not adversely affect *Mest* expression. Longitudinal analyses of bodyweight and body composition in mice fed a HFD shows significantly reduced bodyweight gain and fat mass accumulation in the *Mest*^ApKO mice (Fig 3B and 3C), but no changes in fat-free mass (Fig 3D), compared to the 3 control groups. Reduced bodyweight and adiposity in *Mest*^ApKO mice is consistent with the pheno-types observed for the *Mest*^pKO mice (Fig 2). Both genetic models suggest that MEST facilitates ATE in an obesogenic environment. An additional cohort of mice with *Fabp4*-cre mediated inactivation of *Mest* show similar phenotypic profiles compared to the *Mest*^ApKO mice (S1 Fig).

Metabolic parameters and adipocyte morphology

To prevent aberrant phenotypic measurements due to stress from over-manipulation of the animals, two additional cohorts of *Mest*^pKO mice and littermate WT controls were used to examine diabetic and metabolic parameters. A cohort used to measure glucose (GTT) and insulin tolerance (ITT) showed no significant differences in bodyweight (WT, N = 8, 22.51 ± 0.26 g vs *Mest*^pKO, N = 7, 22.13 ± 0.30 g; p = 0.35) or glucose tolerance (Fig 4A) between chow-fed WT and *Mest*^pKO mice at 8 weeks of age. However, after feeding mice a HFD from 8 to 16 weeks of age, *Mest*^pKO mice showed reduced bodyweight (WT, 38.46 ± 0.96 grams vs *Mest*^pKO, 33.71 ± 1.45 grams; p<0.02) and improved glucose (Fig 4B) and insulin (Fig 4C) tolerance compared to WT littermate controls.

An independent cohort of HFD-fed WT (n = 8) and *Mest*^pKO (n = 8) mice that were sub-jected to indirect calorimetry showed similar differences in both bodyweight and adiposity (Fig 4D and 4E) as previously observed. Surprisingly, caloric intake normalized to fat-free mass (kJ/d/g FFM) measured in mice fed HFD at 8 and 16 weeks of age was similar between WT and *Mest*^pKO mice (Fig 4F) suggesting that differences in food consumption is not a causa-tive factor for the divergence in adiposity between genotypes. Respiratory quotient (RQ) mea-sured in 16 week old mice after feeding a HFD for 8 weeks were identical between genotypes (Fig 4G) and RQ values levels were consistently below 0.8 indicating that fat, as expected due to feeding the mice HFD, is the primary fuel source for both genotypes. Although no signifi-cant differences in energy expenditure (EE; kcal/hr/kg FFM) were noted between genotypes (Fig 4H) at 16 weeks of age, *Mest*^pKO mice did show a ~4–5% elevation in 24 hour EE com-pared to WT mice. Analyses of physical activity based on wheel running at 16 weeks of age shows that *Mest*^pKO mice consistently ran ~15% further (Fig 4I; p≤0.05) and faster (Fig 4J; p≤0.01) than WT mice at night which could at least partially explain the slight increase in EE observed for *Mest*^pKO mice.

Adipocyte morphology for both eWAT and iWAT, determined for the cohort of mice used in the HFD study described in Fig 2 shows that WT mice with high WAT *Mest* expression
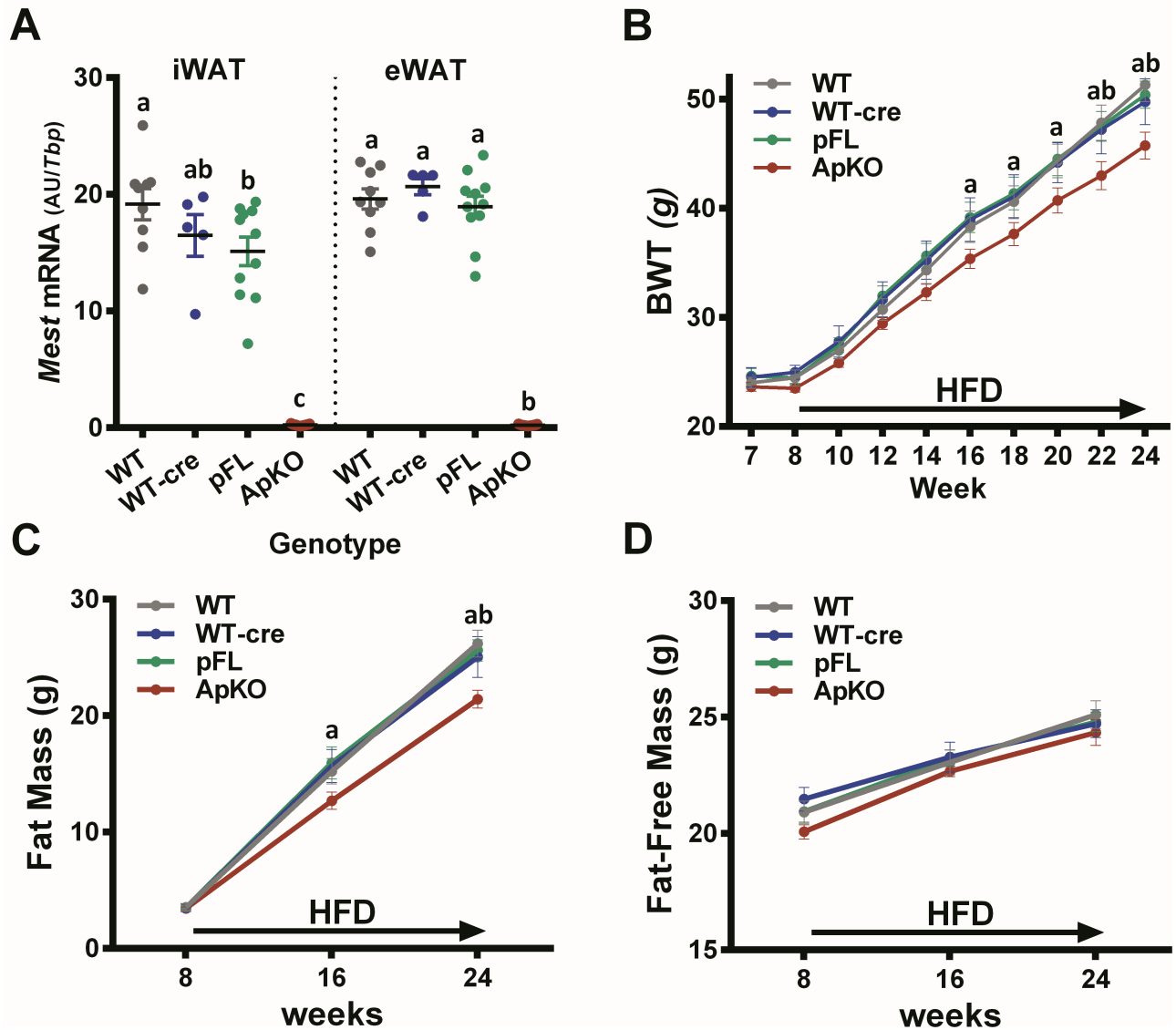
Fig 3. Dietary obesity in mice with *Adipoq*-cre mediated inactivation of *Mest*. (A) *Mest* mRNA expression in inguinal (iWAT) and epididymal (eWAT) white adipose tissue of wildtype (WT; n = 9), WT.*Adipoq*-cre (WT-cre; n = 5), paternal floxed *Mest* (pFL; n = 11) and pFL. *Adipoq*-cre (ApKO; n = 17) mice after being fed a HFD from 8–24 weeks of age. *Mest* mRNA expression measured by TaqMan QRT-PCR is represented as the mean ± SEM of arbitrary units (AU) normalized to TATA-box binding protein (*Tbp*). Significance in *Mest* RNA expression between groups was determined via one-way ANOVA using Tukey's multiple comparisons test. (B) Data shows the longitudinal measurements of bodyweight (BWT) for WT (n = 9), WT-cre (n = 5), pFL (n = 11) and ApKO (n = 17) mice fed a HFD from 8 to 24 weeks of age as indicated by the arrow along the X-axis. (C) Longitudinal measurements of fat mass (g) and (D) fat-free mass (g) measured by DEXA at the times indicated on the X-axis are shown for WT (n = 9), WT-cre (n = 5), pFL (n = 11) and ApKO (n = 17) mice fed a HFD from 8 to 24 weeks of age as indicated by the arrow along the X-axis. (B-D) All data in the longitudinal studies are presented as the mean ± SEM. Significance at each time point of the longitudinal phenotypic analyses was determined by 2-way ANOVA and Tukey's multiple comparisons test. Time points annotated with 'a' and 'b' indicates significant differences between 'ApKO vs pFL' and 'ApKO vs WT'.

https://doi.org/10.1371/journal.pone.0179879.g003

(WT-HM) have significantly larger adipocytes in eWAT ([Fig 5A and 5B](#)) compared to *Mest*[pKO] (p<0.005) or WT mice with low WAT *Mest* expression (WT-LM; p<0.001). Although the size of adipocytes in iWAT ([Fig 5C](#)) was not different between genotypes, the general trend of increased adipocyte hypertrophy in mice within the HM group was evident in both WAT depots. These results are consistent with previous studies using B6 mice fed a HFD
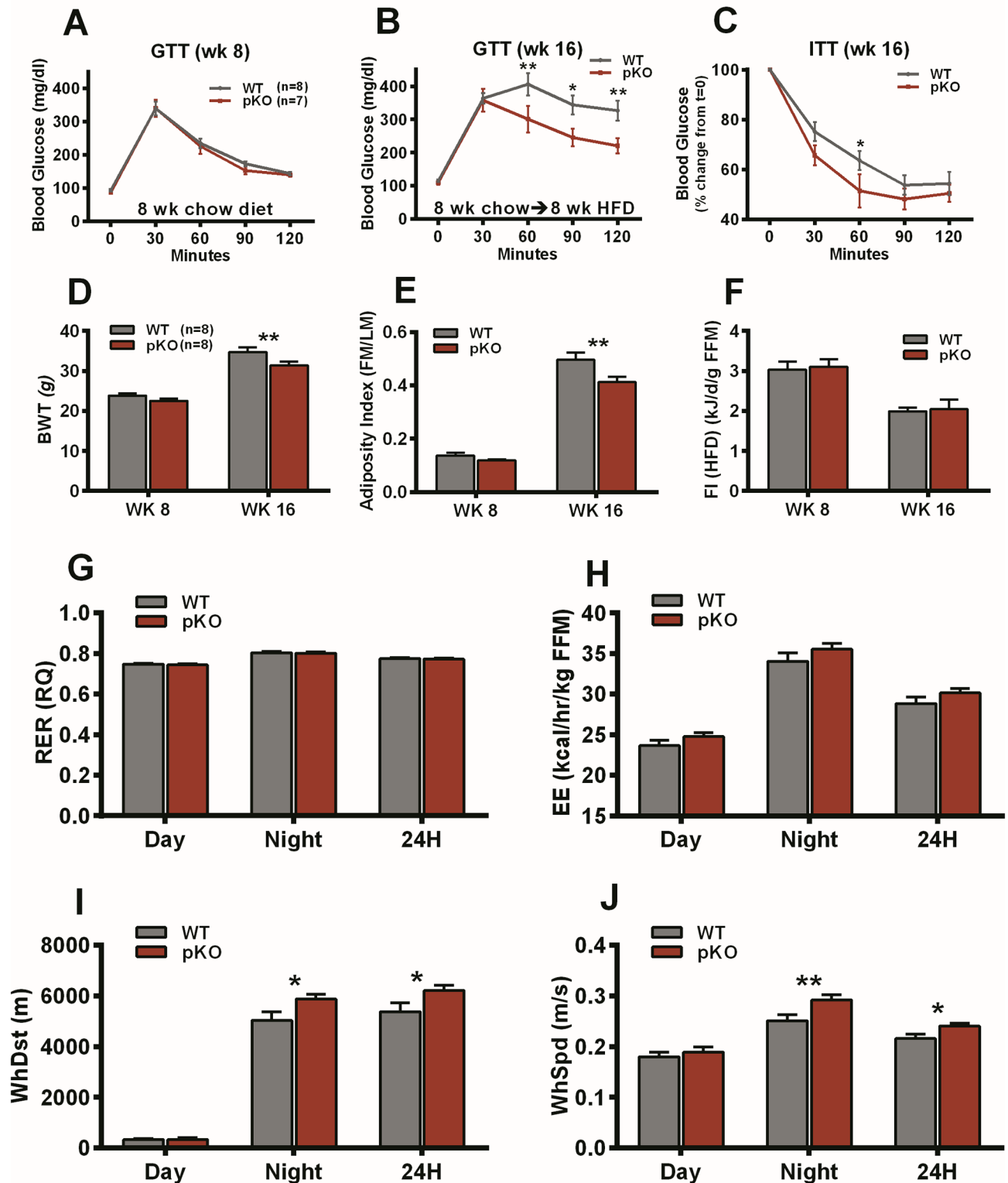
Fig 4. Diabetic and metabolic measurements of mice with inactivated *Mest*. (A) Data shows glucose tolerance test (GTT) of WT (n = 8) and *Mest*[pKO] (pKO) mice (n = 7) fed a chow diet at 8 weeks of age. (B) GTT and (C) insulin tolerance test (ITT) of WT (n = 8) and pKO (n = 7) at 16 weeks of age after feeding mice a high fat diet (HFD) for 8 weeks. (D) Bodyweight (BWT), (E) adiposity index (fat mass/lean mass; FM/LM) and (F) food intake (FI; kJ/day normalized to fat-free mass (FFM) are presented for an additional cohort of WT (n = 8) and pKO (n = 8) mice fed a HFD from 8 to 16 weeks of age that were subjected to indirect calorimetric analyses. Body composition measurements were

performed via DEXA. Indirect calorimetric measurements of (G) respiratory quotient (RQ), (H) energy expenditure (EE), (I) wheel running distance (WhDst) and (J) wheel speed (WhSpd) were performed on mice for 1 week after being fed a HFD for 8 weeks. All data is presented as the mean ± SEM. Significance between groups was determined using two-tailed unpaired parametric t-tests and 1 or 2 asterisks indicate significant P-values of ≤0.05 and ≤0.01 respectively.

that showed a positive correlation between adiposity and adipocyte size with WAT *Mest* mRNA and protein [16].

Gene expression analyses

Gene expression markers for macrophage infiltration/inflammation were used to determine whether improved glucose tolerance in HFD-fed *Mest*[pKO] mice (Fig 4B) is concomitant with reduced inflammatory state of WAT. Gene expression analyses of adipose tissue of the WT, *Mest*[pKO], WT-LM and WT-HM mice used in the HFD study described in Fig 2 showed reduced expression of *Ccl2* (Mcp-1), *Hmox1*, *Itgam* and *Itgax* in eWAT of *Mest*[pKO] compared to the WT and WT-HM mice (Fig 6A, 6B, 6C and 6D). Although differences in the expression of these gene markers between groups were not as prominent in iWAT compared with eWAT, they were consistent with that observed for eWAT except for *Itgax* which showed no differences between groups. The absence of differences in gene expression between the WT-LM and
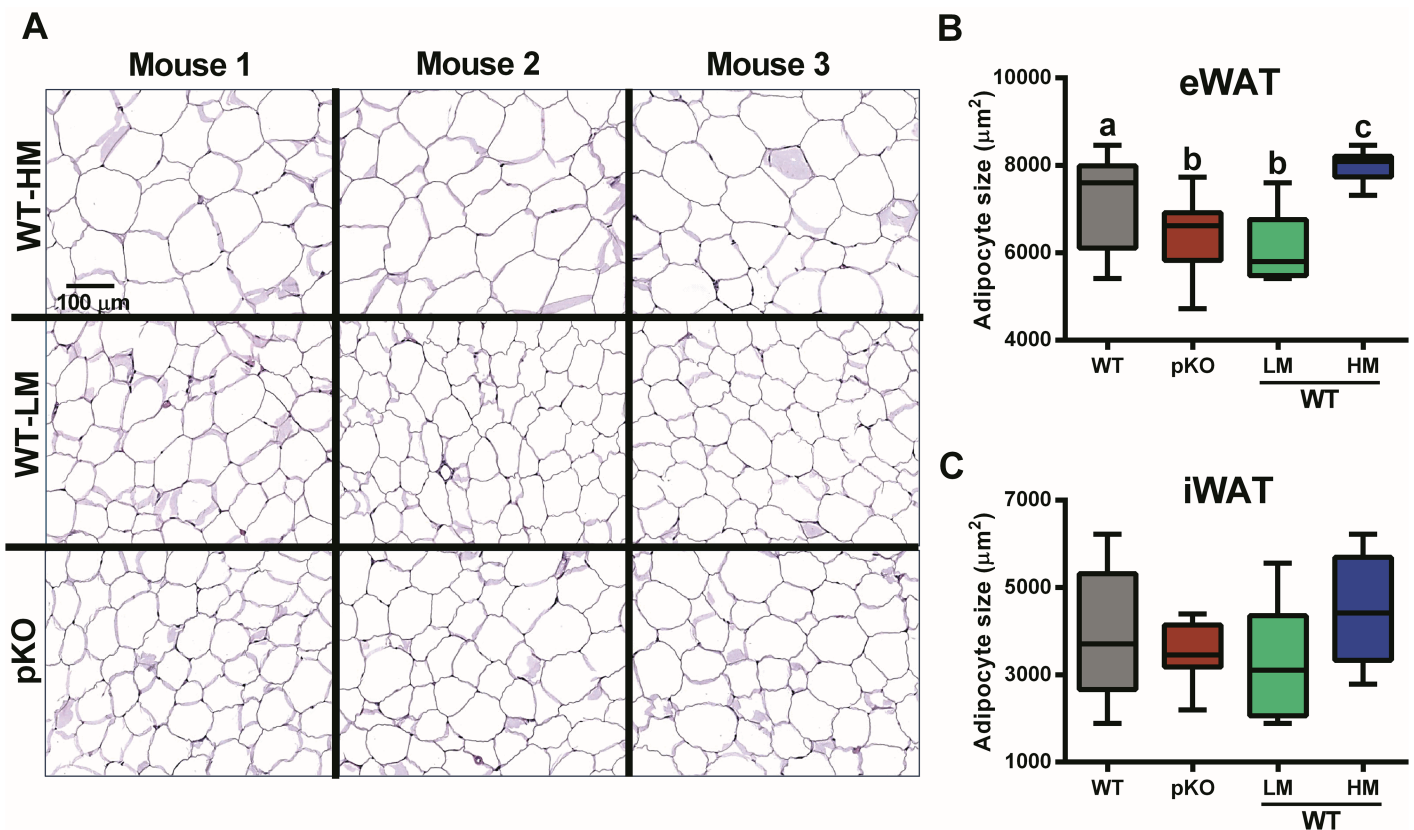
Fig 5. Adipocyte size determination in mice with inactivated *Mest*. (A) A representative image shows variation in the size of adipocytes in eWAT of WT mice with high (WT-HM; n = 3) and low (WT-LM; n = 3) epididymal adipose tissue (eWAT) *Mest* expression and *Mest*[pKO] (pKO) mice (n = 3). (B and C) Box and whisker graphs show the median and range of adipocyte sizes determined morphometrically for WT (n = 17), pKO (n = 10), WT-LM (n = 6) and WT-HM (n = 6) mice for both eWAT and inguinal adipose tissue (iWAT). Significance between groups was determined using two-tailed unpaired parametric t-tests. Datasets annotated with the same letter indicate no significant differences between groups.
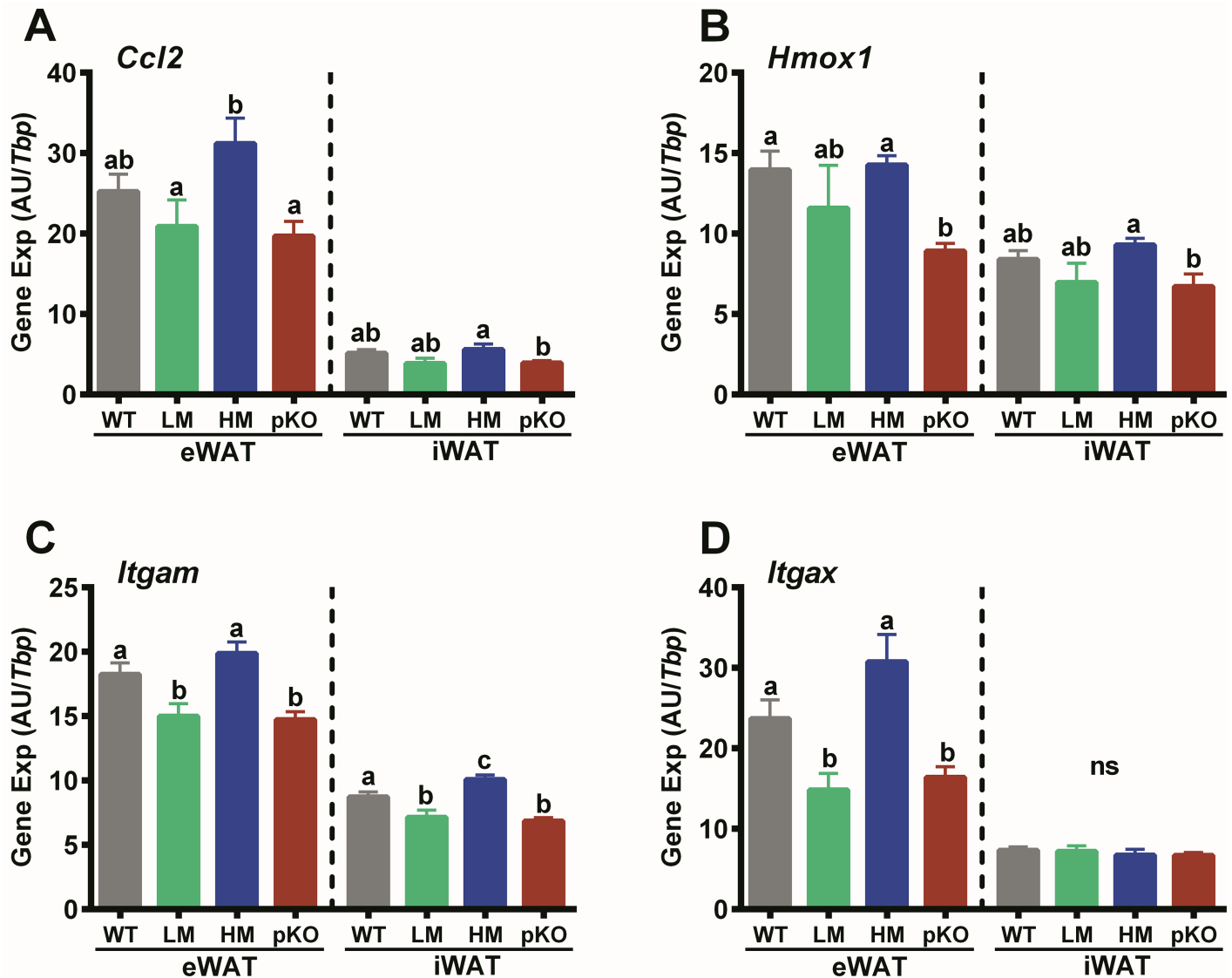
Fig 6. Inflammatory genes in WAT of mice with inactivated *Mest*. A, B, C and D show expression of gene markers for inflammation and macrophage infiltration in WAT of WT and *Mest*^**pKO** (pKO) mice. Gene expression was determined via TaqMan qRT-PCR in total RNA from eWAT and iWAT of wildtype (WT; n = 17), mice with a paternal inactivation of *Mest* (pKO; n = 10) and subgroups of WT mice with low (LM; n = 6) and high (HM; n = 6) WAT *Mest* expression after being fed a HFD from 8–16 weeks of age. Gene expression is represented as arbitrary units (AU) normalized to *Tbp* and presented as the mean ± SEM. Statistical analysis between genotypes within each WAT depot was performed using two-tailed unpaired parametric t-tests and datasets annotated with the same letter indicate no significant differences between groups.

Mest^**pKO** mice suggest that changes in gene expression in *Mest*^**pKO** mice are associated with the reduction of ATE and suppression of inflammation. Furthermore, the analyses of hepatic gene expression in WT vs *Mest*^**pKO** mice show no differences in the expression of *Fas* (WT; 10.09 ± 0.75 vs *Mest*^**pKO**; 10.47 ± 1.53 AU/Tbp; p = 0.83) and *Scd1* (WT; 11.55 ± 0.70 vs *Mest*^**pKO**; 11.93 ± 1.22 AU/Tbp; p = 0.79), genes involved in hepatic *de novo* lipogenesis that have been shown to be positively associated with hepatic steatosis [49–52]. These data indicate that reduced ATE in *Mest*^**pKO** mice does not result in the development of a lipodystrophic state characterized by excessive hepatic accumulation of lipid.

Activation of both canonical and non-canonical Wnt signaling has been shown to inhibit adipogenesis, mediate adipose tissue development and expansion and promote adipose tissue inflammation in obesogenic conditions [53–55]. Because previous studies have shown that adipose tissue *Mest* mRNA expression is positively associated with a subset of genes that include Wnt signaling inhibitors (i.e. *Sfrp5* and *Nkd1*), in addition to the *Tgfb*-pathway mediator *Bmp3* and the serine protease inhibitor *Serpine1* [10, 13, 16], an analyses of this subset of genes in eWAT and iWAT of WT and *Mest*^**pKO** mice from the HFD study described in Fig 2 was performed to determine effects of *Mest* inactivation on their expression. Surprisingly, inactivation of *Mest* did not significantly alter WAT expression of *Sfrp5*, *Bmp3*, *Nkd1* and *Serpine1* (Fig 7B, 7C, 7D and 7E) with levels of expression comparable to WT-LM mice. However, consistent with previous studies [10, 13, 16], WT-HM mice did show elevated levels of *Sfrp5*, *Bmp3*, *Nkd1* and *Serpine1* expression compared with WT-LM mice for both WAT depots (Fig 7B, 7C, 7D and 7E). Additional regression analyses of gene expression in WAT of the 17 WT mice used in the HFD-study in Fig 2 showed significant correlations between *Mest* vs *Sfrp5* ($p = 0.00067$), *Bmp3* ($p = 0.013$) and *Nkd1* ($p = 0.031$) in eWAT; and, between *Mest* vs *Sfrp5* ($p = 0.000025$), *Bmp3* ($p = 0.013$), *Nkd1* ($p = 0.0081$) and *Serpine1* ($p = 0.0052$) in iWAT. No differences in *Pparg* expression were observed between groups (Fig 7F) and *Pparg* mRNA in WAT was not associated with WAT *Mest* as shown in previous studies [7].
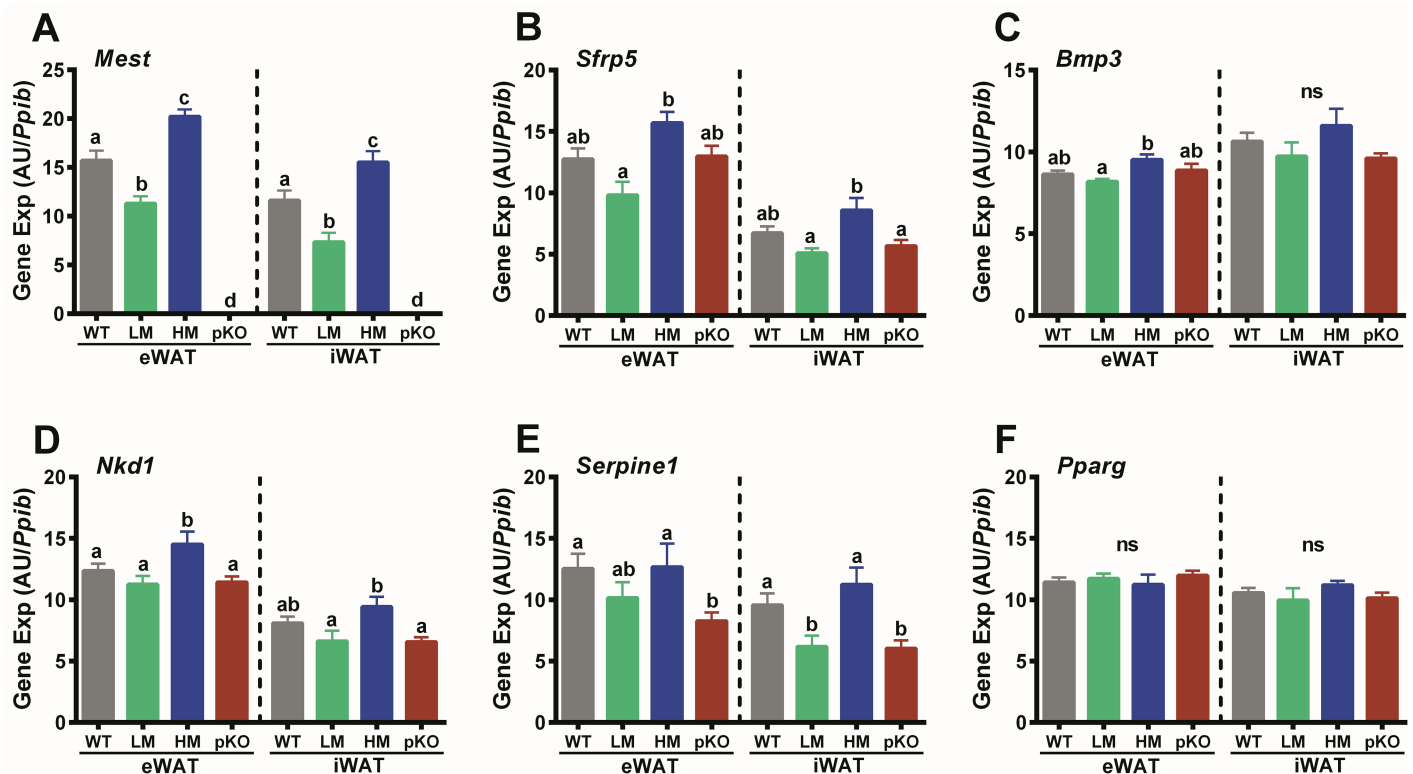
Fig 7. WAT gene expression in mice with inactivated *Mest*. (A) Data shows expression of *Mest*, (B) *Sfrp5*, (C) *Bmp3*, (D) *Nkd1*, (E) *Serpine1*, and (F) *Pparg* in epididymal (eWAT) and inguinal (iWAT) white adipose tissue of wildtype (WT; n = 17) mice with a paternal inactivation of *Mest* (pKO; n = 10) and subgroups of WT mice with low (LM; n = 6) and high (HM; n = 6) WAT *Mest* expression after being fed a HFD from 8–16 weeks of age. Gene expression was determined via TaqMan qRT-PCR in total RNA from eWAT and iWAT and represented as arbitrary units (AU) normalized to cyclophilin b (*Ppib*). Gene expression is presented as the mean ± SEM and significance between groups was determined using two-tailed unpaired parametric t-tests. Datasets annotated with the same letter indicate no significant differences between groups.

https://doi.org/10.1371/journal.pone.0179879.g007

A global analysis of gene expression via ABI SOLiD SAGE sequencing was used to identify genes and genetic pathways that are dysregulated in adipose tissue of mice with a targeted inactivation of *Mest* (Fig 8). Gene profiles for eWAT were analyzed for 6 WT and 5 *Mest*^{pKO} mice selected from the cohort used in the HFD study in Fig 2. Adiposity indices (FM/LM ratio) of the WT mice were significantly higher than *Mest*^{pKO} mice (WT, 0.724 ± 0.030; *Mest*^{pKO}, 0.571 ± 0.019; p = 0.003) after the 8 weeks of HFD. A Venn diagram (Fig 8A) shows surprisingly few genes from the 15,453 gene targets detected in eWAT to have significantly higher (n = 27) or lower expression (n = 9) in WT vs *Mest*^{pKO} mice when FDR-adjusted to P<0.1 (S1 Table). *Mest*, as expected, was significantly reduced >15-fold in eWAT of *Mest*^{pKO} mice and TaqMan qRT-PCR validation showed undetectable (reduced >100-fold) levels of *Mest* in eWAT and iWAT of *Mest*^{pKO} mice (Table 1). Analyses of 14 additional selected genes with RNA from the individual eWAT samples used for ABI SOLiD SAGE sequencing via qRT-PCR showed significant and consistent differences between WT and *Mest*^{pKO} mice in the expression of 10 genes whereas 2 genes (*Negr1*, *Mrap*) showed no significant differences between groups and 2 genes (*Plagl2*, *Tph2*) could not be detected (Table 1). Additional analyses of eWAT RNA from the entire cohort of 17-WT and 10- *Mest*^{pKO} mice also showed comparable patterns of expression for the 10 differentially-expressed genes with the global and sample validation studies (Table 1). Importantly, 7 of the 10 genes showed similar expression patterns for both iWAT and eWAT whereas the expression of 3 genes (*Gsta3*, *Ucp2* and *Ces1f*) only showed differences in eWAT.

Ontology and enrichment analyses of the 27 genes with reduced expression in eWAT of *Mest*^{pKO} mice showed associations with several biological processes including cation transport (*Tfr2*, *Atp6v0a1*, *Atp6v0d2*, *Slc5a7*, *Ccdc109b* and *Trdn*; P<10^{-4}), regulation of growth of symbiont in host (*Lbp*, *Irf8*; P<10^{-3}), myeloid leukocyte activation (*Lbp*, *Pirb*, *Ubd*; P<10^{-3}) and acute phase response (*Lbp*, *Hp*; P<10^{-3}); however, none of the associations were significant after FDR correction. Genes more highly expressed in eWAT of *Mest*^{pKO} showed modest association with mycotoxin/aflatoxin catabolism and metabolism (*Gsta3*; P<10^{-3}) and monoterpenoid metabolism (*Cyp2e1*; P<10^{-3}). Further enrichment analyses performed on non-FDR-adjusted gene sets with a P-value cutoff of ≤ 0.05 and a minimum of 50 sequence tags for each mRNA in at least one of the groups identified 695 gene targets that were differentially expressed in eWAT of WT vs *Mest*^{pKO} mice (S2 Table). The 395 genes with reduced expression in eWAT of *Mest*^{pKO} mice showed highly significant associations with immune system processes (Padjusted <10^{-10}) including defense, immune, inflammatory and stress responses whereas genes with increased expression in eWAT of *Mest*^{pKO} mice (n = 301) showed enrichment for single-organism metabolic processes (Padjusted<10^{-3}) including oxidation-reduction, organic acid metabolism; and, fatty acid, acyl-CoA, thioester and monocarboxylic acid metabolism (Fig 8B). An examination of the expression of the mature mouse macrophage gene marker F4/80 (*Emr1*; *Adgre1*), and gene markers that delineate classically (M1) versus alternatively (M2) macrophage subtypes [56] only showed significantly elevated expression for the M1 macrophage marker *Gpr18* (p = 0.04) and M2 macrophage marker *Egr2* (p = 0.02) in eWAT of WT mice. No differences in expression between genotypes were observed for F4/80, *Cd38*, *Fpr2*, *Cd163*, *Cd68* and *Myc*.

Adipogenic differentiation of Ear-derived mesenchymal stem cells

In vivo inactivation of *Mest* both globally and in adipocytes was shown to reduce adiposity (Figs 2 and 3); therefore, studies were initiated to determine whether similar effects of *Mest* inactivation can be observed in an adipogenic population of primary ear-derived mesenchymal progenitor cells (EMSC) from mice [57]. Results showed that EMSC from *Mest*^{gKO} mice
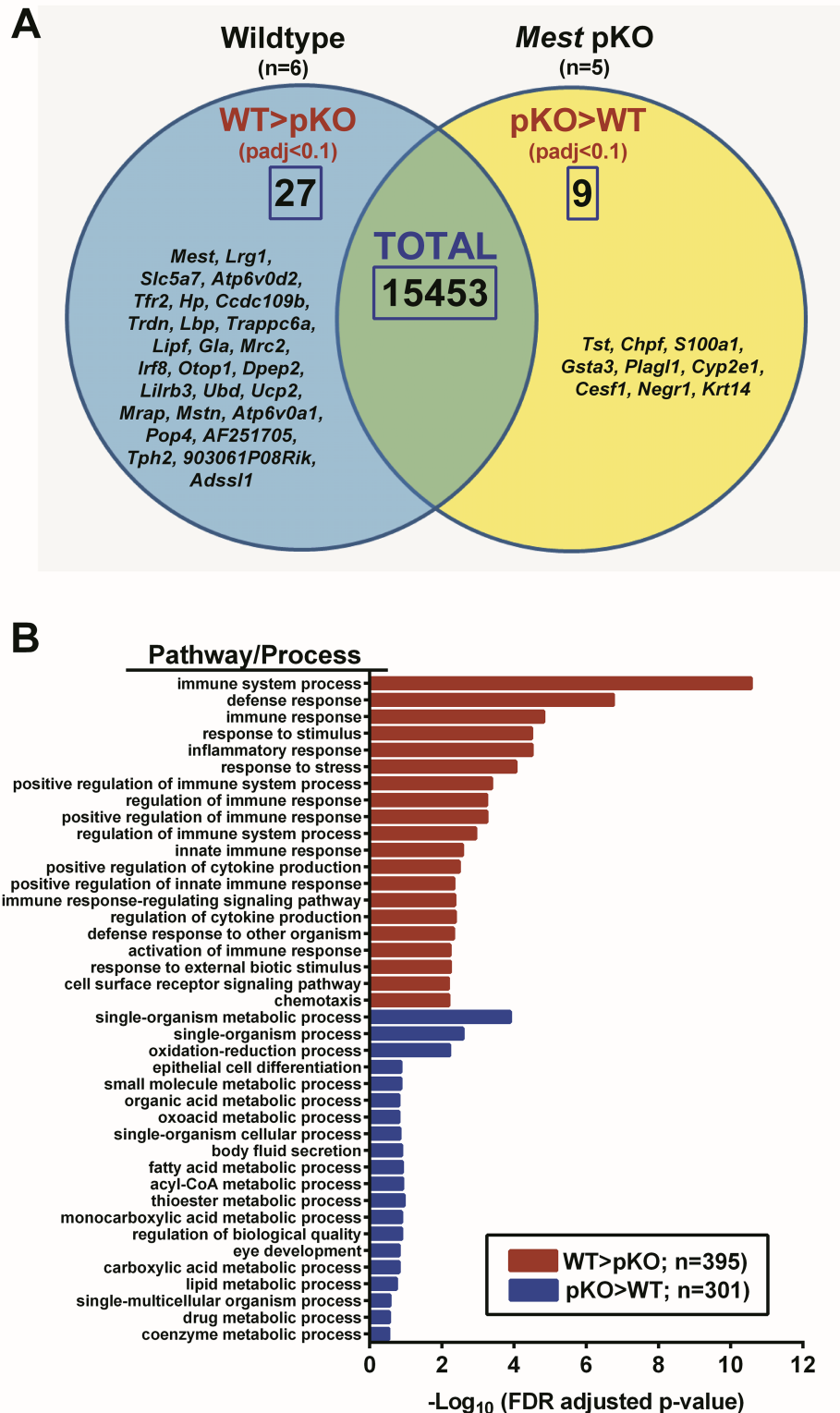
Fig 8. Global analyses of gene expression in eWAT of mice with global inactivation of *Mest*. (A) A Venn diagram represents a summary of ABI SoLID SAGE analyses of differentially expressed genes in eWAT of 6-wildtype (WT) and 5- *Mest*^pKO (pKO) mice fed a high fat diet from 8 to 16 weeks of age. Differentially expressed genes have a false discovery rate (FDR) adjusted P-value ≤ 0.1 and at least one genotype with ≥ 50 sequenced tags per gene. (B) The bar graph represents pathway analyses of 695 genes differentially expressed in eWAT of WT versus *Mest*^pKO mice that have non-adjusted P-values of ≤ 0.05 and at least one genotype with ≥ 50 sequenced tags per gene (S2 Table).

Table 1. Validation of differentially-expressed genes in eWAT of WT and pKO mice.

Gene	ABI SOLiD SAGE Analyses			qRT-PCR validation			
	FC (WT/pKO)	pval[a]	padj[b]	FC(WT/pKO) SAGE RNA	pval[c] (ttest)	FC (17-WT/10-pKO) RNA; eWAT/iWAT	pval (ttest)[c] RNA; eWAT/iWAT
Mest	15.09	1.6E-65	2.5E-61	>100	3.5E-06	>100/>100	1.3E-12/3.3E-09
Lrg1	2.26	9.6E-09	4.4E-05	1.57	2.6E-04	1.40/1.35	0.0019/0.0015
Slc5a7	2.21	1.4E-08	4.4E-05	2.10	6.9E-05	1.79/1.65	2.4E-04/0.0030
Atp6v0d2	2.69	1.2E-08	4.4E-05	2.29	0.0072	1.86/1.83	0.0023/0.0014
Tfr2	2.71	1.2E-08	4.4E-05	2.29	0.00040	1.77/1.84	0.0010/0.0011
Gsta3	0.52	5.4E-06	0.0070	0.61	0.021	0.77/1.01	0.016/0.89
Lbp	1.87	7.2E-06	0.0076	1.42	0.0044	1.27/1.53	0.0013/0.0017
Lipf	2.16	7.3E-06	0.0076	2.57	0.0032	1.81/2.37	0.0020/0.0015
Mrc2	1.93	1.2E-05	0.011	2.12	0.0043	1.61/1.66	0.0032/0.0021
Plagl1	0.55	2.0E-05	0.016	ND	ND	ND	ND
Ucp2	1.67	8.9E-05	0.053	1.43	0.0082	1.34/1.10	0.0057/0.13
Ces1f	0.46	8.0E-05	0.053	0.52	0.0032	0.71/0.97	0.010/0.64
Negr1	0.58	1.2E-04	0.062	0.78	0.11	0.92/1.02	0.33/0.76
Mrap	1.71	1.1E-04	0.062	1.18	0.12	1.13/1.12	0.16/0.44
Tph2	4.52	2.1E-04	0.094	ND	ND	ND	ND

eWAT, epididymal white adipose tissue; iWAT, inguinal white adipose tissue; WT, wildtype mice; pKO, *Mest*[pKO] mice; FC, fold change; SAGE, serial analyses of gene expression; ND, not detected.

[a]p-values were calculated using SAM as described in Materials and Methods.

[b]p-values were adjusted for false discovery rate using the Benjamini-Hochberg method.

[c]p-values were determined using two-tailed unpaired parametric t-tests.

https://doi.org/10.1371/journal.pone.0179879.t001

were comparable in their capacity for adipogenic differentiation and accumulation of lipids compared to EMSC from WT mice as indicated by the panels showing oil red O (ORO) staining of lipids and crystal violet (CV) staining of cell nuclei (Fig 9A); and, in longitudinal profiles of lipogenesis measured by spectrophotometric determination of ORO in two independent experiments (Fig 9B and 9C). Although these results are somewhat contradictory to what is observed with *in vivo* studies, one possible explanation for the lack of effect of *Mest* inactivation in EMSC adipogenesis could be that cellular access to abundant nutrients and robust expression of lipid biosynthetic glycerol- and acyl-glycerol phosphate acyl transferases (GPATs and AGPATs) simply overwhelms the contribution MEST might have in facilitating lipid accumulation. By using an approach similar to one that used siRNA knockdown of GPAM in HEK293 cells to confirm GPAT-function for AGPAT6 [58], now renamed GPAT4, it was hypothesized that attenuation of GPAT/AGPAT function in EMSC might allow the contribution of MEST in lipid accumulation in EMSC undergoing adipogenesis to emerge. To test this possibility, EMSC were transduced with a lentiviral (LV) construct expressing shRNA against *Gpat4*, a glycerol-3-phosphate O-acyltransferase that catalyzes the acylation of glycerol-3-phosphate in the first and rate limiting step of *de novo* triacylglycerol and glycerophospholipid synthesis. *Gpat4* was selected because, like *Mest*, it is localized within the endoplasmic reticulum (ER) [59] and is expressed during adipogenic differentiation of EMSC derived from both WT and *Mest*[gKO] mice (Fig 9D and 9E). Expression of *Gpat4* in EMSC from WT mice transduced with LV shRNA against *Gpat4* (GP4KD) was reduced ~65–70% 5 days after initiation of adipogenic differentiation (Fig 9D). The expression of *Agpat2* and *Gpat3*, which have 42% and 67% coding sequence identity with *Gpat4* and are highly expressed in EMSC during adipogenic differentiation, are unaffected in the GP4KD EMSC (Fig 9D). Interestingly, *Mest* expression was
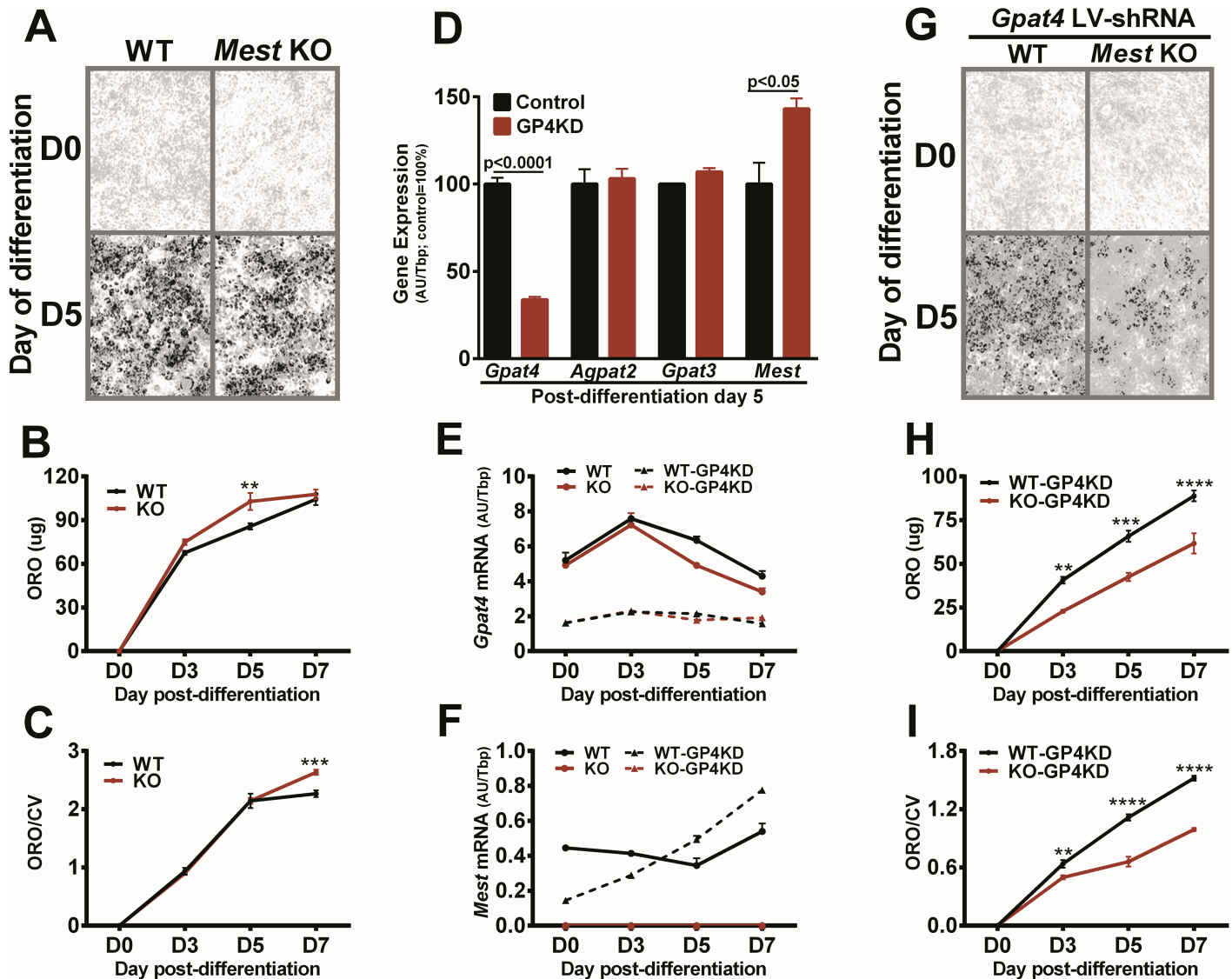
Fig 9. *In vitro* analysis of adipogenesis and effects of *Gpat4*-knockdown on ear-derived mesenchymal progenitor cells from wildtype and *Mest* KO mice. (A) Oil red O (ORO) staining of lipid is shown in representative 10X (gray-scale) microscopic images of ear-derived mesenchymal progenitor cells (EMSC) from WT and homozygous *Mest* knockout (KO) mice prior to (D0) and after 5 days (D5) of adipogenic differentiation. (B) Graph represents spectrophotometric measurements of eluted ORO (ug) during 7 days of adipogenic differentiation using 3–4 replicate cultures of EMSC from WT and *Mest* KO mice for each time point on the X-axis. (C) Data shows an additional independent experiment using 3–4 replicate cultures of EMSC from WT and *Mest* KO mice at each time point during adipogenic differentiation that were stained with ORO and counterstained with crystal violet (CV) to normalize for cell number. (D) Figure shows mRNA expression of *Gpat4*, *Agpat2*, *Gpat3* and *Mest* measured by qRT-PCR in WT EMSC in the absence (Control; n = 3) or presence of lentiviral shRNA knockdown of *Gpat4* (GP4KD; n = 3) at post-adipogenic differentiation day 5. Gene expression data is presented as arbitrary units normalized to *Tbp* (AU/*Tbp*). Significance in gene expression between control and GP4KD cells was determined using two-tailed unpaired parametric t-tests and p-values between groups are indicated. (E) and (F) show *Gpat4* and *Mest* mRNA expression in duplicate samples for WT and *Mest* KO EMSC in the absence or presence of GP4KD during adipogenic differentiation from D0 to D7. (G) ORO staining of lipid is shown in representative 10X (gray-scale) microscopic images of WT and *Mest* KO EMSC in the presence of GP4KD prior to (D0) and after 5 days (D5) of adipogenic differentiation. (H) Spectrophotometric profiles of eluted ORO during 7 days of adipogenic differentiation are shown for 3–4 replicates of WT and *Mest* KO EMSC after GP4KD are shown for each time point on the X-axis. (I) Data shows an additional independent experiment using 3–4 replicate cultures of EMSC from WT and *Mest* KO mice after GP4KD at each time point during adipogenic differentiation that were stained with ORO and counterstained with CV to normalize for cell number. Significance at each time point of adipogenic differentiation (B, C, H and I) was determined by 2-way ANOVA and Sidak's multiple comparisons test. Datasets with 2, 3 or 4 asterisks indicate p-values of <0.01, <0.001 and <0.0001 respectively.

https://doi.org/10.1371/journal.pone.0179879.g009

modestly increased ~30% in GP4KD EMSC which suggests that its activation is a possible compensatory response to the attenuation of GPAT4 function. An independent longitudinal study using EMSC from WT and *Mest*^{gKO} mice in the absence or presence of GP4KD shows comparable temporal patterns of *Gpat4* expression during 7 days of adipogenic differentiation among genotypes which was significantly attenuated by the GP4KD (Fig 9E). *Mest* expression in WT GP4KD EMSC was initially lower than WT EMSC during the first 3 days after adipogenic differentiation was initiated (i.e. D0-D3), but was higher than WT EMSC by day 5 post-differentiation (Fig 9F) which is consistent with previous results (Fig 9D). While GP4KD transduced WT and *Mest*^{gKO} EMSC showed highly attenuated lipogenesis (Fig 9G) compared to non-transduced cells (Fig 9A), GP4KD was significantly more effective in mitigating lipogenesis in *Mest*^{gKO} EMSC compared with WT EMSC as observed in the ORO/CV stained image (Fig 9G) and in the spectrophotometric measurements of ORO stained lipids in two independent longitudinal studies (Fig 9H and 9I). These data suggest that intact MEST function in WT EMSC diminishes GP4KD-mediated reductions of lipogenesis and supports a role for MEST in facilitating lipid accumulation.

Discussion

Since adipose tissue *Mest* was found to be positively associated with variable development of diet-induced obesity within a genetically homogeneous population of mice [10], a number of studies by our laboratory and others have utilized *Mest* as a sensitive biological indicator for adipocyte hypertrophy and fat expansion [7, 14, 16, 21, 60]. The initial characterization of mice with a targeted inactivation of *Mest* on a mixed genetic background (*Mest*^{tm1Lef}) did not describe adiposity-related phenotypes; however, these mice were smaller than control animals, had high rates of early post-natal lethality and showed abnormal maternal behavior [43]. Subsequent analyses of a subset of 9-month old *Mest*^{tm1Lef} mice on a mixed B6/129 background showed modestly reduced bodyweights and fat pad weights suggesting a role for MEST in the storage of lipid in adipocytes [16]. To avoid problems associated with abnormal maternal behavior and post-natal lethality in *Mest*-deficient mice, which would confound the interpretation of MEST function in diet-induced obesity and adipose tissue expansion (ATE), we generated an isogenic (C57BL/6J) mouse model with *loxP* sites flanking the 3rd exon of *Mest* to selectively inactivate *Mest* in a tissue-specific manner. Surprisingly, the creation of mice with Ella-cre-mediated global inactivation of *Mest* using our targeted model, unlike the *Mest*^{tm1Lef} mice [43], did not result in increased risk of early post-natal lethality, reduced post-natal longitudinal growth, or abnormal maternal behavioral phenotypes. The reasons for differences between our targeted *Mest* mouse model and *Mest*^{tm1Lef} are not well understood but could be due to differences in the genetic background of the mice, the gene targeting construct, or mutation(s) in the host ES cell used for targeting [61]. Recently it was reported that backcrossing targeted *Mest*^{tm1Lef} mice 5 generations onto a129/SVJ background also eliminated the early postnatal lethality and maternal behavioral phenotypes of mice with a paternal inactivation of *Mest*; however, the explanation why this occurred was not clearly defined [62].

A microRNA (*miR-335*) suggested to have a role in the regulation of lipid metabolism, adipogenesis, adipose tissue inflammation and chondrogenesis [47, 48, 63] is located within the 2nd intron of *Mest* TV2 (Fig 1D) and only ~595 bp upstream (5') from the loxP/NEO cassette used to generate the targeted *Mest* allele. The regulation of miR-335 is complex with some studies suggesting that it is a paternally expressed imprinted microRNA that is co-regulated with *Mest* whereas others suggest that it can be regulated via its own promoter [48, 64]. Since it is plausible that perturbed *miR-335* function could modify ATE in our mouse model, it was necessary to determine whether *miR-335* is dysregulated in mice with targeted *Mest*. Analyses

of *miRNA-335-5p* expression in iWAT of 6–7 day old mice, at a time when fat accretion is rapid and *Mest* is highly expressed [16], showed comparable levels of *miR-335* for all genotypes (Fig 1E) with no evidence for dysregulation of *miR-335* in mice with inactivated *Mest*. Normal *miR-335* expression in mice with a targeted allele of *Mest* suggests that phenotypic differences primarily result from loss of MEST function.

HFD-fed mice with inactivation of *Mest* on the paternal allele (*Mest*^PKO) showed significantly reduced bodyweight (Fig 2A), adiposity (Fig 2B and 2C), adipocyte hypertrophy (Fig 4) and improved glucose and insulin tolerance (Fig 4B and 4C); but, relatively few differences in metabolic parameters measured by indirect calorimetry (Fig 4G, 4H, 4I and 4J) compared to WT littermate controls. Although a reduction in bodyweight of just a little over 4 grams between male *Mest*^PKO and WT mice after being fed a HFD for 8 weeks appears to be modest, this would be equivalent to a 177 vs 200 pound individual with ~75% (~17.3 lbs) of the additional bodyweight being fat mass. Additional studies using *Mest*^PFL mice with either *Adipoq-* or *Fabp4*-cre mediated inactivation of the paternal *Mest* allele primarily in adipocytes (Fig 3; S1 Fig) showed similar reductions in both bodyweight and adiposity compared to their respective littermate controls suggesting that inactivation of *Mest* in adipocytes is predominantly responsible for the observed differences in adiposity related phenotypes between genotypes.

A predicted complication in assessing phenotypic differences between WT mice and mice with global or adipose tissue specific inactivation of *Mest* was the expected variability in the development of obesity within the WT cohort and its positive association with WAT MEST [7, 10, 16]. This was in fact the case and was exemplified by the analyses of tertiles (n = 6) of WT mice with the lowest (WT-LM) and highest (WT-HM) eWAT *Mest* mRNA expression (Fig 2D and 2E). Our analyses showed that differences in bodyweight and adiposity were more pronounced when comparing *Mest*^PKO with WT-HM mice and were consistent with previous studies of interindividual variation of *Mest* in the absence of genetic heterogeneity. When tertiles for male WT mice based on eWAT *Mest* expression are extrapolated to human body weight, WT-HM and WT-LM would weigh 215 vs183 pounds respectively. The lack of difference observed for bodyweight, adiposity, and adipocyte hypertrophy between WT-LM and *Mest*^PKO mice fed a HFD suggests that 'basal' levels of ATE do not require MEST. Additionally, studies showing increased adipocyte hypertrophy in mice with transgenic overexpression of *Mest* [20] coupled with high interindividual variability in WAT *Mest* expression in a genetically homogeneous population of mice [10, 16, 65] supports the premise that MEST could be an 'epigenetically' regulated rheostat for the control of ATE beyond defined basal levels established by the genetic background.

A concern with the ablation of *Mest* in a murine mouse model was that it could reduce the capacity for WAT to expand in an obesogenic environment leading to adipose dysfunction, ectopic accumulation of hepatic and intramuscular lipid, and impaired insulin sensitivity similar to that observed in lipodystrophy [66, 67]. However, *Mest*^PKO mice fed a HFD for 8 weeks showed markedly improved glucose homeostasis compared with WT controls (Fig 4B and 4C) which suggest that the suppression of ATE in *Mest*^PKO mice does not adversely affect metabolic health of WAT. These observations are supported by reduced WAT expression of markers for inflammation, hypoxia and macrophage infiltration in *Mest*^PKO and WT-LM mice compared to WT-HM mice (Fig 6) and lack of differences in hepatic expression of genes shown to be associated with the development of hepatic steatosis [49–52]. Data suggests that improved glucose tolerance is at least partially caused by reduced ATE in mice with inactivated or low WAT *Mest* expression. Improved glucose metabolism in association with reduced adipocyte lipid accumulation in mice with deficient *Mest*, caused by reduced adipocyte lipid accumulation shows similarity to the maintenance of normal glucose metabolism by caloric

restriction; or, by mechanisms that enhance energy expenditure such as physical activity or cold-activated thermogenesis [68–73].

Although WT mice accrued significantly more bodyweight and adiposity than *Mest*[PKO] mice after being fed a HFD for 8 weeks (Fig 4D and 4E), there were no differences in caloric intake between genotypes when measured during the initial (wk 8) and final week (wk 16) of high fat feeding (Fig 4F). Since indirect calorimetric measurements showed a consistent but non-significant (~4–5%) increase in energy expenditure for *Mest*[PKO] mice during the day and night (Fig 4H) as well as significantly increased nighttime activity (Fig 4I and 4J), it is possible that these small differences in energy expenditure during the 8-week longitudinal study could contribute to some of the phenotypic differences in bodyweight and adiposity between genotypes.

Genes (i.e. *Sfrp5*, *Bmp3*, *Nkd1* and *Serpine1*) expressed in WAT previously identified as being positively correlated with WAT *Mest* mRNA and variable development of adiposity in a genetically homogeneous population of mice fed obesogenic diet [7, 10, 16] were not significantly effected in WAT of *Mest*[PKO] mice (Fig 7B, 7C, 7D and 7E). However, consistent with previous studies, analyses of WAT gene expression in the WT mice used in the HFD study in Fig 2 showed significant positive associations between eWAT *Mest* vs *Sfrp5*, *Bmp3* and *Nkd1*; and, between iWAT *Mest* vs *Sfrp5*, *Bmp3*, *Nkd1* and *Serpine1*. Since these genes were expressed at similar levels in WAT of HFD-fed *Mest*[PKO] and WT-LM mice (Fig 7A, 7B, 7C, 7D and 7E), both of which show comparable weight gain and adiposity (Fig 2E and 2F), this suggests that differences in adiposity rather than WAT MEST affects their expression.

RNA-Seq analyses performed with RNA from eWAT of WT and *Mest*[PKO] mice to gain insight into gene pathways and mechanisms related to MEST function revealed relatively few differences in gene expression (~36 genes) between genotypes when corrected for FDR at a p-value of <0.1 (Fig 8A) which suggests that ablation of *Mest* has relatively modest effects on gene expression in adipose tissue. This is an exciting feature of the association of reduced MEST and ATE with improved glucose/insulin metabolism because, unlike many other anti-obesity therapies, it provides encouragement that targeting the MEST pathway to reduce ATE may have a minimal number of side effects. Pathway analyses of genes with reduced and increased expression in eWAT of *Mest*[PKO] mice (Fig 8A) showed modest associations with immune system-based pathways and metabolism/catabolism of toxins, respectively. The use of a broader set of genes with less stringent criteria for significance (S2 Table) in the gene ontology enrichment analyses also showed genes with reduced expression in eWAT of HFD-fed *Mest*[PKO] mice to be associated with immune system processes (Fig 8B), including inflammation, which is consistent with improved glucose tolerance and insulin sensitivity in these mice. Genes more highly expressed in eWAT of *Mest*[PKO] were categorized within multiple metabolic processes including those associated with metabolism of acyl-CoA, fatty acids and lipids (Fig 8B) and included a subset of carboxylesterases (*Ces1d*, *Ces1f*), carnitine palmitoyltransferase 2 (*Cpt2*) and glycerol-3-phosphate acyltransferases (*Gpat4*, *Gpat3*; S2 Table). Since elevated *Mest* is associated with increased adiposity, the increased expression of lipid biosynthetic genes in the absence of MEST may reflect a compensatory response. GPAT4, an integral membrane protein is important for the first step in catalyzing triglyceride synthesis and has been suggested to diffuse from the endoplasmic reticulum (ER) to lipid droplets via membrane bridges [74]. Since evidence suggests that MEST is localized within the ER [16, 20, 27], it's plausible that interactions between MEST and GPAT4, or with other ER-localized GPATs or AGPATs, could facilitate triglyceride synthesis and storage in adipocytes. Studies are currently underway to delineate temporal patterns of MEST localization within the ER and its proximity to nascent lipid droplet formation.

Catalytic promiscuity and moonlighting are common among α/β-hydrolase fold proteins thus making it difficult to associate a specific catalytic function for MEST based on sequence homology [75–77]. Although the precise catalytic mechanism for MEST has not been defined, evidence showing a role for MEST in augmenting ATE and lipid accumulation in adipocytes [7, 16, 20] coupled with its intracellular localization within the ER [16, 20, 27] and the presence of a catalytic triad associated with proteases, lipases and acyltransferases within its peptide sequence [24, 26], all suggest that MEST acts to facilitate the accumulation of lipid in adipocytes.

The observation that mesenchymal progenitor cells (EMSC) derived from mice with a targeted inactivation of *Mest* (*Mest*[gKO]) showed no difference in adipogenic potential and lipid accumulation compared to WT EMSC (Fig 9A, 9B and 9C) is contradictory to results showing increased lipid accumulation in 3T3-L1 adipocytes with transgenic overexpression of *Mest* [20]; and, underscores the complexity involved in understanding MEST function using *in vitro* models. However, in lentiviral shRNA knockdown of GPAT4, a gene whose inactivation in mice causes subdermal lipodystrophy and reduced diet-induced obesity [78], in both WT and *Mest*[gKO] EMSC resulted in the emergence of differences in adipogenesis between the two genotypes with EMSC derived from *Mest*[gKO] mice showing significantly reduced lipid accumulation compared to WT EMSC (Fig 9G, 9H and 9I). These data provide strong evidence that MEST at physiological levels may augment lipid accumulation and storage during adipogenic differentiation by its own endogenous acyltransferase activity, interact with or stabilize proteins associated with fatty acid uptake or lipid droplet formation, or reduce adipogenesis-suppressing intracellular levels of EET [35–37] via endogenous epoxide hydrolase activity. Proteomic and lipodomic studies are needed to further delineate the precise catalytic mechanisms associated with MEST and its role in mediating ATE and glucose homeostasis in WAT.

In summary, our data shows that reduced diet-induced ATE in MEST-deficient mice diminishes expression of markers of hypoxia and inflammation in WAT which leads to improved glucose tolerance and insulin sensitivity. Since minimal additional physiological effects are observed in mice with inactivation of *Mest*, an intervention that represses the function of MEST, or its associated pathway, could be a feasible strategy to mitigate obesity and the inception of T2D.

Methods

Gene targeting

A cre/*lox*P system was used to create mice with global and conditional inactivation of mesoderm specific transcript *(Mest)*. DNA amplified from a C57BL/6J genomic BAC clone (RP24-211g11) was used to generate a targeting vector with *lox*P sites flanking exon 3 of *Mest* transcript variant/protein isoform 2 (NM_008590.2). A third *lox*P site flanking a NEO cassette (G418 resistance) 5' of exon 3 was included as a selectable marker. Targeted C57BL/6J embryonic stem cells carrying the conditional floxed allele were introduced into C57BL/6J-Tyrc-2J host blastocysts and chimeric progeny crossed with C57BL/6J-Tyrc-2J mice to generate mice heterozygous for the targeted allele. The presence and correct orientation of the 3 *lox*P sites with respect to *Mest* exon 3 and the NEO cassette were confirmed via PCR. Generation of mice with global inactivation of *Mest* and with a floxed *Mest* exon 3 in the absence of the NEO cassette was achieved by crossing mice carrying the targeted allele to *Ella*-cre mice which has restricted expression of cre recombinase under the control of the adenoviral *Ella* promoter in oocytes and in preimplantation embryos [79]. Progeny that show positive PCR amplification patterns that correspond to a complete deletion of the floxed region and/or deletion of the

NEO cassette were backcrossed to C57BL/6J mice to ensure germline transmission of the mutation and removal of the *Ella*-cre transgene.

Animals and study design

Since *Mest* is almost exclusively expressed from the paternally-derived allele in adult mice, experimental cohorts of mice with a paternal inactivation of Mest (*Mest*$^{\text{PKO}}$) were generated by crossing wildtype (WT) C57BL/6J female mice with male mice heterozygous for the inactivated (KO) *Mest* allele on the maternal allele (*Mest*$^{\text{mKO}}$). This cross yields equal ratios of WT and *Mest*$^{\text{PKO}}$ mice. Complete knockout of *Mest* in tissues of *Mest*$^{\text{PKO}}$ mice have been verified by both gene expression and Western blot analysis (Fig 1B and 1C). Longitudinal dietary obesity studies were performed using male WT and *Mest*$^{\text{PKO}}$ mice because male C57BL/6J has greater susceptibility for the development of diet-induced obesity than females. Experimental cohorts of mice to study the conditional inactivation of *Mest* were generated via crosses between female mice that are hemizygous for either the *Fabp4*-cre (B6.Cg-Tg (Fabp4-cre) 1Rev/J; JAX Stock# 005069) or *Adipoq*-cre (B6;FVB-Tg(Adipoq-cre)1Evdr/J; JAX Stock# 010803) transgenes with male mice containing either a maternal (*Mest*$^{\text{mFL}}$) or paternal (*Mest*$^{\text{pFL}}$) floxed allele for *Mest*. The resulting genotypes will include mice with *Fabp4*- or Adipoq-cre inactivation of the paternal allele for *Mest* (*Mest*$^{\text{FpKO}}$ or *Mest*$^{\text{ApKO}}$ respectively) and control groups consisting of WT, WT-cre (*Fabp4*- or *Adipoq*-cre) and *Mest*$^{\text{pFL}}$ mice. Prior to use in generating experimental mice, the *Adipoq*-cre transgenic mice were crossed to C57BL/6J for several subsequent generations to eliminate potential genomic contribution from the FVB strain. Genomic analyses of the Adipoq-cre using a 1449 SNP marker panel (Taconic, Germantown, NY) confirms 99.79% C57BL/6J with the only residual genome of FVB located between ~83.5 and ~92.1 mb on mouse *Chr 9*, the putative genomic insertion site of the *Adipoq*-cre transgene [80].

The animals were maintained in a temperature-controlled room (23˚C) with a 12-h light/12-hr dark cycle. For experiments performed at Pennington Biomedical Research Center, the mice were reared under conventional conditions and fed PicoLab Rodent Diet 20 (Lab Diet; 13 kcal% fat) after weaning. For experiments conducted at Maine Medical Center Research Institute Animal Facility, the mice were kept in a barrier facility and given 2018 Teklad Global 18% Protein Rodent Diet (Harlan; 18 kcal% fat) post-weaning. For dietary obesity studies mice were singly-housed at 7 weeks of age and then fed a high fat diet (HFD; D12331, Research Diets; 58 kcal% fat; 23.26 kJ/g) starting a 8 weeks of age for 8–16 weeks as indicated for each study cohort. The design used for the dietary obesity studies for each of the cohorts of mice are shown in S3 Table. Upon completion of the studies, all mice were sacrificed by anesthesia with isoflurane followed by cervical dislocation according to accepted guidelines and tissues were harvested for analyses. All animal experiments and methods were approved by the Institutional Animal Care and Use Committee at The Pennington Biomedical Research Center (Baton Rouge, LA) and The Maine Medical Center Research Institute (Scarborough, ME) in accordance with National Institutes of Health guidelines for care and use of laboratory animals.

Glucose and insulin tolerance tests

Glucose tolerance test (GTT) was performed in 7 week old male mice prior to initiation of high fat diet and repeated after 8 weeks on high fat diet. Mice were fasted overnight and administered 2 g/kg BW glucose intraperitoneally (IP). Blood glucose levels were determined using Accu-check Aviva plus system (Roche Diagnostics). Insulin tolerance test was conducted

in mice fed high fat diet for 8 weeks. Mice were fasted for 6 hours and injected with human recombinant insulin (Humulin-R, Eli Lilly and Company) at a dose of 1.5 kg/BW IP.

Indirect calorimetry

The Promethion Metabolic Cage System (Sable Systems) was used for indirect calorimetry. The mice were acclimated to the system for 12-hrs followed by 72-hr data collection.

Determination of body composition

Nuclear magnetic resonance. Body composition (body fat, lean mass and free fluid) was analyzed by Minispec NMR (Bruker) which allowed for non-invasive, serial body composition measurements in the mouse. The Minispec uses the contrasting hydrogen density and/or hydrogen spin properties from adipose tissue and muscle for estimating body composition. A quality control check of NMR parameters using a standard provided by the manufacturer was performed at the beginning of each day of testing.

Dual-energy X-ray absorptiometry. Mice were scanned using the Lunar PIXImus densitometer (GE Medical Lunar; DEXA). Whole-body and femoral areal bone mineral density, and body composition excluding the head were determined in each mouse under isoflurane anesthesia (IsoFlo, Abbot Labs). The Piximus was calibrated at the beginning of each day of testing using a phantom according to the manufacturer's instructions.

Histology and morphometrics of white adipose tissue

Inguinal (iWAT) and epididymal (eWAT) adipose tissue were fixed in Bouin's solution (Sigma-Aldrich), and paraffin-embedded sections were stained with H & E. Adipocyte area and size distribution were analyzed using Image J software at specific parameters to measure area of each adipocyte based on size and exclusion limits.

Mest transcript variants

RNA was extracted from eWAT and iWAT of wild-type mice (Mest$^{+/+}$) homogenized in TriReagent (Molecular Research Center, Inc.) and then purified using RNeasy Mini Kit and RNase-free DNAse (Qiagen). Isolated RNA was protected from RNAse contamination with SUPERase-In (Life Technologies). RNA quantity and quality was determined using Nanodrop 1000 spectrophotometer. Specific primers against the *Mest* transcript variants 1(TV1; forward: 5'-CCCTGTGATCCGCAATCCT-3'; reverse: 5'-ACTACTGTCTGCATTTGGGCTATG-3'), 2 (TV2; forward: 5'-GCGGCATGGGATAATGC-3'; reverse: 5'-CTACTTGGACCCACCACTCTCT-3') and 3 (TV3; forward: 5'-GGGTAGAGAGAAAAAGTGTGGAA-3'; reverse: 5'-CCTCTAAGGAACAGCGACTTC-3') were designed using Primer Express software v3.0.1 (Life Technologies) to yield amplicons ranging from 72 to 99 bp. White adipose tissue cDNA was synthesized using High-Capacity cDNA Reverse Transcription Kit (Life Technologies). Quantitative PCR was performed using 20 ng cDNA input and yield was compared between 25, 30 and 36 PCR cycles. PCR products were resolved using 3% GenePure LE agarose (ISC Bioexpress) in 1X TBE running buffer at 80 volts for 20 mins. Gel image was obtained using Gel-Doc-ItTS2 Imaging System (UVP).

Quantitative reverse transcription PCR

Expression of mRNA. Quantitative reverse transcription-PCR was performed using total RNA with specific primers and probes (S3 Table) designed using Primer Express software v3.0.1 (Life Technologies) essentially as previously described [16] except that a BioRad CFX

Real-Time System was also used for analyses. TaqMan probes (Biosearch Technologies) were used for gene quantification using TaqMan® RNA-to-CT 1-Step Kit (Life Technologies). Gene expression data were normalized to level of cyclophilin b (*Ppib*), or TATA box binding protein (*Tbp*). In addition, the total nanograms of input RNA/reaction was quantified using Qubit HS RNA Assay Kit (Life Technologies) and can be used to normalize gene expression by RNA input if necessary.

Expression of miRNA. Total RNA including miRNAs was isolated from white adipose tissue using miRNeasy mini kit (Qiagen). cDNA synthesis was performed using the TaqMan® MicroRNA Reverse Transcription Kit and TaqMan miRNA specific primers (Life Technologies) for mmu-miR-335-5p, mmu-miR-335-3p and snoRNA202 (NCBI Accession #AF357327). The cDNA was amplified using the TaqMan Universal Mastermix II, no UNG and TaqMan Small RNA Assay (Life Technologies). Quantitive PCR was performed using the CFX384 Real Time PCR detection system (BioRad). Relative abundance of miR-335 was quantified using the $2^{-\Delta\Delta CT}$ method using snoRNA202 for normalization of expression.

Western blot analyses

Total tissue lysate from eWAT and iWAT were prepared in RIPA buffer containing 1% protease, phosphatase I and phosphatase II inhibitors (Sigma). Protein content was determined using Sigma BCA protein assay kit. Proteins were resolved on 10% SDS-PAGE gel and after separation electro-transferred to PVDF (Immobilon-P, EMD Millipore) or nitrocellulose (Hybond-ECL, GE Healthcare) membranes. Blots were incubated in antibodies against MEST (1:5000) and GAPDH (1:1000, ABCAM ab9484). Bands were visualized and quantified using the Odyssey imaging system (Li-Cor Bioscience).

In vitro cell culture

Experimental cohorts for *in vitro* experiments were generated by intercrossing *Mest* heterozygous mice to generate WT (+/+), *Mest*^{**pKO**} (+/KO) and *Mest*^{**gKO**} (KO/KO) mice. Ear mesenchymal stem cells (EMSCs) were isolated from WT and *Mest*^{**gKO**} mice as previously described [57]. Cells were cultured in 5% CO_2 and maintained in DMEM/F-12 (Life Technologies) supplemented with 10% FBS (Life Technologies) supplemented with Primocin as an antibiotic (InVivoGen), and 10 ng/ml recombinant bFGF (PeproTech). To induce adipocyte differentiation, recombinant bFGF was removed and replaced with 10% FBS with 0.5 mM methylisobutylxanthine, 1 uM dexamethasone, 5 ug/ml insulin, and 5 uM troglitazone. On day 2, cells were fed 5 ug/ml insulin plus 5 uM troglitazone. On day 4 and every 2 days thereafter, cells were fed with 15% FBS. Lipid droplets were visualized using Oil Red O staining. Cells were washed with PBS followed by fixation with 10% neutral buffered formalin for 10 min. The cells were then washed once in dH_2O and incubated in 60% isopropanol for 5 min. The isopropanol was removed and followed by an incubation in Oil Red O staining solution (0.35% Oil Red O in 60% isopropanol) for 10 min, washed once in 60% isopropanol and 3X for 10 min with dH_2O. Oil Red O dye was eluted in 100% isopropanol for 15 minutes. The degree of adipogenic differentiation was quantified spectrophotometrically by measuring absorbance at 490 nm. A standard curve with known amounts of Oil Red O dye (ug/ml) was used to quantify lipid as total ug of Oil Red O eluted. After elution of Oil Red O dye, cells were then washed 1X with 100% isopropanol followed by dH_2O and subsequently used for quantifying relative cell number by nuclear staining with crystal violet. Relative cell number was measured by staining cells with 0.05% crystal violet in deionized H_2O for 5 minutes. The cells were then washed 3X for 10 min with dH_2O then lysed in 1% SDS. Crystal violet in the 1% SDS lysate was measured

at an absorbance of 560 nm a standard curve with known amounts of crystal violet (ug/ml) was used to quantify relative cell number and to normalize Oil Red O eluted from cells.

Gene knockdown

Five short-hairpin RNA (shRNA) constructs against *Gpat4* (Agpat6) in lentiviral vector pLKO.1 were obtained from Sigma-Aldrich. For knockdown experiments, the construct chosen was TRCN0000099245. According to the manufacturer's protocol, EMSC were transduced in maintenance medium in the presence of polybrene (Sigma-Aldrich). Transduction was performed at MOI = 2. After overnight incubation, virus-containing media was removed and standard culture media was added. Cells were allowed to expand for 48 hours and then selection was initiated using puromycin (Sigma-Aldrich) at 4 ug/ml. Puromycin-resistant cells were expanded until P6 and then seeded in 12-well plates at a density of 100,000 cells per well. Prior to lentiviral transduction, a titration was performed to determine the minimum concentration of puromycin required to cause complete cell death after 3–5 days. Cells were harvested for gene expression, Oil Red O and crystal violet staining.

SOLiD SAGE analyses

SAGE gene expression profiling was performed with next-generation sequencing using the Life Technologies 5500XL SOLiD system. RNA was isolated from tissues using TRI Reagent; quantified and quality was determined using an Agilent 2100 Bioanalyzer. RNA was transcribed into cDNA via priming at the poly A+ tail. Double-stranded cDNA was digested with *Nla*III restriction enzyme and ligated to adaptors containing an EcoP15L restriction site. Digestion was performed with *EcoP*15L and ligation of "bar code" oligonucleotides that specifically label each sample, and subsequent PCR amplification yielded a library for sequencing where each gene was represented with a 3'-expression tag. The alignment of sequence tags back to a reference genome was performed using a modified version of the Applied Biosystems SOLiD™ SAGE™ Analysis Software v1.10 that was installed, modified to meet stringent mapping criteria, and extensively tested in-house. RNA isolated from eWAT of 6 independent wildtype control mice and 5 *Mest*[pKO] mice were used for preparation of libraries and sequencing analyses. Raw count files were analyzed by the R/Bioconductor program DE-Seq31; significance and predictive analyses were performed using SAM (Significance Analysis of Microarrays; http://www-stat.stanford.edu/~tibs/SAM/index.html) and PAM (Prediction Analysis for Microarrays; http://statweb.stanford.edu/~tibs/PAM/index.html) respectively [81, 82]. P-values were adjusted for false discovery rate using the Benjamini-Hochberg method [83]. Pairwise analysis and hierarchical clustering of samples was performed using Bioconductor edgeR Version 3.2.3 and JMP Genomics respectively. Raw sequencing files from ABI SOLiD SAGE analyses have been deposited in NCBI's Gene Expression Omnibus (GEO; https://www.ncbi.nlm.nih.gov/geo/) with the accession number GSE96968.

Statistics

Statistical calculations were performed using GraphPad Prism software V.6 and Microsoft Excel 2010. Differences between 2 groups were calculated using two-tailed unpaired parametric t-test with confidence level at 95%. Significance among multiple groups was calculated with ordinary one-way ANOVA followed by Tukey's multiple comparisons test with an alpha of 0.5 or by the Fisher's LSD test as indicated. Significance at each time point of longitudinal phenotypic datasets was determined using 2-way ANOVA with Holm-Sidak multiple comparisons test. Data is presented as the mean ± SEM. $P < 0.05$ was considered to be significant.

Ethics statement

The use of murine models for the studies presented in the submitted manuscript was approved by the Institutional Animal Care and Use Committees (IACUC) at the Pennington Biomedical Research Center and the Maine Medical Center Research Institutes.

Supporting information

S1 Fig. Dietary obesity in mice with *Fabp4*- cre mediated inactivation of *Mest*. (A) *Mest* mRNA expression in inguinal (iWAT) and epididymal (eWAT) white adipose tissue of wild-type (WT; n = 8), WT.*Fabp4*-cre (WT-cre; n = 11), paternal floxed *Mest* (pFL; n = 6) and pFL. *Fabp4*-cre (FpKO; n = 12) mice after being fed a high fat diet (HFD) from 8 to 20 weeks of age. *Mest* mRNA expression measured by TaqMan QRT-PCR is represented as the mean ± SEM arbitrary units (AU) normalized to cyclophilin b (*Ppib*). Significance in *Mest* RNA expression between groups was determined via one-way ANOVA using Tukey's multiple comparisons test. (B) Data shows the longitudinal measurements of bodyweight (BWT) for WT (n = 8), WT-cre (n = 11), pFL (n = 6) and FpKO (n = 12) mice fed a HFD from 8 to 20 weeks of age as indicated by the arrow along the X-axis. (C) Longitudinal measurements of adiposity index; (D) fat-free mass (g) and (E) fat mass (g) measured by NMR at the times indicated on the X-axis are shown for WT (n = 8), WT-cre (n = 11), pFL (n = 6) and FpKO (n = 12) mice fed a HFD from 8 to 20 weeks of age as indicated by the arrow along the X-axis. (B-E) All data in the longitudinal studies are presented as the mean ± SEM. Significance at each time point of the longitudinal phenotypic analyses was determined by 2-way ANOVA and Tukey's multiple comparisons test. Time points annotated with 'a', 'b', 'c', and 'd' indicate significant differences between 'FpKO vs pFL'; 'FpKO vs WT'; 'FpKO vs WT-cre' and 'FpKO vs all genotypes respectively. (F) Data shows morphometric analyses of adipocyte size in eWAT in WT (n = 8), WT-cre (n = 11), pFL (n = 6) and FpKO (n = 12) mice. Two-tailed unpaired parametric t-tests were used to determine significant differences in adipocyte size (F) between genotypes. Datasets annotated with the same letter indicate no significant differences between groups.
(TIF)

S1 Table. Differential gene expression in eWAT: WT vs pKO; FDR padj ≤ 0.1.
(DOCX)

S2 Table. Differential gene expression in eWAT; WT vs pKO; pvalue ≤ 0.05.
(DOCX)

S3 Table. Murine cohorts and study design.
(DOCX)

S4 Table. Primer and probe sets: qRT-PCR.
(DOCX)

Acknowledgments

Author Contributions

Conceptualization: RAK LPK.

Formal analysis: RAK RPA.

Funding acquisition: RAK.

Investigation: RAK RPA JM.

Methodology: RLM JZ RAK RPA.

Project administration: RAK.

Visualization: RAK.

Writing – original draft: RAK.

Writing – review & editing: LPK RPA.

References

1. Bouchard C, Tremblay A, Despres JP, Nadeau A, Lupien PJ, Theriault G, et al. The response to long-term overfeeding in identical twins. The New England journal of medicine. 1990; 322(21):1477–82. https://doi.org/10.1056/NEJM199005243222101 PMID: 2336074

2. Stunkard AJ, Harris JR, Pedersen NL, McClearn GE. The body-mass index of twins who have been reared apart. The New England journal of medicine. 1990; 322(21):1483–7. https://doi.org/10.1056/NEJM199005243222102 PMID: 2336075

3. Locke AE, Kahali B, Berndt SI, Justice AE, Pers TH, Day FR, et al. Genetic studies of body mass index yield new insights for obesity biology. Nature. 2015; 518(7538):197–206. https://doi.org/10.1038/nature14177 PMID: 25673413;

4. Bouchard C. Defining the genetic architecture of the predisposition to obesity: a challenging but not insurmountable task. The American journal of clinical nutrition. 2010; 91(1):5–6. Epub 2009/11/27. https://doi.org/10.3945/ajcn.2009.28933 PMID: 19939981.

5. Jaenisch R, Bird A. Epigenetic regulation of gene expression: how the genome integrates intrinsic and environmental signals. Nature genetics. 2003; 33 Suppl:245–54. PMID: 12610534. https://doi.org/10.1038/ng1089

6. Li S, Zhao JH, Luan J, Luben RN, Rodwell SA, Khaw KT, et al. Cumulative effects and predictive value of common obesity-susceptibility variants identified by genome-wide association studies. The American journal of clinical nutrition. 2010; 91(1):184–90. Epub 2009/10/09. https://doi.org/10.3945/ajcn.2009.28403 PMID: 19812171.

7. Anunciado-Koza RP, Manuel J, Koza RA. Molecular correlates of fat mass expansion in C57BL/6J mice after short-term exposure to dietary fat. Annals of the New York Academy of Sciences. 2016; 1363:50–8. https://doi.org/10.1111/nyas.12958 PMID: 26647164;

8. Burcelin R, Crivelli V, Dacosta A, Roy-Tirelli A, Thorens B. Heterogeneous metabolic adaptation of C57BL/6J mice to high-fat diet. Am J Physiol Endocrinol Metab. 2002; 282(4):E834–42. PMID: 11882503. https://doi.org/10.1152/ajpendo.00332.2001

9. Koza RA, Flurkey K, Graunke DM, Braun C, Pan HJ, Reifsnyder PC, et al. Contributions of dysregulated energy metabolism to type 2 diabetes development in NZO/H1Lt mice with polygenic obesity. Metabolism. 2004; 53(6):799–808. PMID: 15164332.

10. Koza RA, Nikonova L, Hogan J, Rim JS, Mendoza T, Faulk C, et al. Changes in gene expression foreshadow diet-induced obesity in genetically identical mice. PLoS Genet. 2006; 2(5):e81. PMID: 16733553. https://doi.org/10.1371/journal.pgen.0020081

11. Yang Y, Smith DL Jr., Keating KD, Allison DB, Nagy TR. Variations in body weight, food intake and body composition after long-term high-fat diet feeding in C57BL/6J mice. Obesity (Silver Spring). 2014; 22(10):2147–55. https://doi.org/10.1002/oby.20811 PMID: 24942674;

12. de Fourmestraux V, Neubauer H, Poussin C, Farmer P, Falquet L, Burcelin R, et al. Transcript profiling suggests that differential metabolic adaptation of mice to a high fat diet is associated with changes in liver to muscle lipid fluxes. J Biol Chem. 2004; 279(49):50743–53. PMID: 15377667. https://doi.org/10.1074/jbc.M408014200

13. Kozak LP, Newman S, Chao PM, Mendoza T, Koza RA. The early nutritional environment of mice determines the capacity for adipose tissue expansion by modulating genes of caveolae structure. PLoS One. 2010; 5(6):e11015. Epub 2010/06/25. https://doi.org/10.1371/journal.pone.0011015 PMID: 20574519.

14. Chu DT, Malinowska E, Gawronska-Kozak B, Kozak LP. Expression of adipocyte biomarkers in a primary cell culture models reflects preweaning adipobiology. J Biol Chem. 2014; 289(26):18478–88. https://doi.org/10.1074/jbc.M114.555821 PMID: 24808178;

15. Kozak LP, Koza RA, Anunciado-Koza R, Mendoza T, Newman S. Inherent plasticity of brown adipogenesis in white fat of mice allows for recovery from effects of post-natal malnutrition. PLoS One. 2012; 7 (2):e30392. https://doi.org/10.1371/journal.pone.0030392 PMID: 22383960;

16. Nikonova L, Koza RA, Mendoza T, Chao PM, Curley JP, Kozak LP. Mesoderm-specific transcript is associated with fat mass expansion in response to a positive energy balance. FASEB journal: official publication of the Federation of American Societies for Experimental Biology. 2008; 22(11):3925–37. Epub 2008/07/23. https://doi.org/10.1096/fj.08-108266 PMID: 18644838.

17. Moraes RC, Blondet A, Birkenkamp-Demtroeder K, Tirard J, Orntoft TF, Gertler A, et al. Study of the alteration of gene expression in adipose tissue of diet-induced obese mice by microarray and reverse transcription-polymerase chain reaction analyses. Endocrinology. 2003; 144(11):4773–82. PMID: 12960083. https://doi.org/10.1210/en.2003-0456

18. Soukas A, Cohen P, Socci ND, Friedman JM. Leptin-specific patterns of gene expression in white adipose tissue. Genes & development. 2000; 14(8):963–80. 0010783168.

19. Soukas A, Socci ND, Saatkamp BD, Novelli S, Friedman JM. Distinct transcriptional profiles of adipogenesis in vivo and in vitro. J Biol Chem. 2001; 276(36):34167–74. PMID: 11445576.

20. Takahashi M, Kamei Y, Ezaki O. Mest/Peg1 imprinted gene enlarges adipocytes and is a marker of adipocyte size. Am J Physiol Endocrinol Metab. 2005; 288(1):E117–24. https://doi.org/10.1152/ajpendo.00244.2004 PMID: 15353408.

21. Voigt A, Ribot J, Sabater AG, Palou A, Bonet ML, Klaus S. Identification of Mest/Peg1 gene expression as a predictive biomarker of adipose tissue expansion sensitive to dietary anti-obesity interventions. Genes & nutrition. 2015; 10(5):477. https://doi.org/10.1007/s12263-015-0477-z PMID: 26143179;

22. Bluher M. Adipose tissue dysfunction in obesity. Experimental and clinical endocrinology & diabetes: official journal, German Society of Endocrinology [and] German Diabetes Association. 2009; 117 (6):241–50. https://doi.org/10.1055/s-0029-1192044 PMID: 19358089.

23. Rutkowski JM, Stern JH, Scherer PE. The cell biology of fat expansion. The Journal of cell biology. 2015; 208(5):501–12. https://doi.org/10.1083/jcb.201409063 PMID: 25733711;

24. Holmquist M. Alpha/Beta-hydrolase fold enzymes: structures, functions and mechanisms. Curr Protein Pept Sci. 2000; 1(2):209–35. PMID: 12369917.

25. Ollis DL, Cheah E, Cygler M, Dijkstra B, Frolow F, Franken SM, et al. The alpha/beta hydrolase fold. Protein Eng. 1992; 5(3):197–211. PMID: 1409539.

26. Carter P, Wells JA. Dissecting the catalytic triad of a serine protease. Nature. 1988; 332(6164):564–8. Epub 1988/04/07. https://doi.org/10.1038/332564a0 PMID: 3282170.

27. Jung H, Lee SK, Jho EH. Mest/Peg1 inhibits Wnt signalling through regulation of LRP6 glycosylation. The Biochemical journal. 2011; 436(2):263–9. https://doi.org/10.1042/BJ20101512 PMID: 21375506.

28. Decker M, Arand M, Cronin A. Mammalian epoxide hydrolases in xenobiotic metabolism and signalling. Arch Toxicol. 2009; 83(4):297–318. Epub 2009/04/03. https://doi.org/10.1007/s00204-009-0416-0 PMID: 19340413.

29. Kaneko-Ishino T, Kuroiwa Y, Miyoshi N, Kohda T, Suzuki R, Yokoyama M, et al. Peg1/Mest imprinted gene on chromosome 6 identified by cDNA subtraction hybridization. Nature genetics. 1995; 11(1):52–9. PMID: 7550314. https://doi.org/10.1038/ng0995-52

30. Cowart LA, Wei S, Hsu MH, Johnson EF, Krishna MU, Falck JR, et al. The CYP4A isoforms hydroxylate epoxyeicosatrienoic acids to form high affinity peroxisome proliferator-activated receptor ligands. J Biol Chem. 2002; 277(38):35105–12. Epub 2002/07/19. https://doi.org/10.1074/jbc.M201575200 PMID: 12124379.

31. Fang X, Hu S, Watanabe T, Weintraub NL, Snyder GD, Yao J, et al. Activation of peroxisome proliferator-activated receptor alpha by substituted urea-derived soluble epoxide hydrolase inhibitors. J Pharmacol Exp Ther. 2005; 314(1):260–70. Epub 2005/03/31. https://doi.org/10.1124/jpet.105.085605 PMID: 15798002.

32. Fang X, Hu S, Xu B, Snyder GD, Harmon S, Yao J, et al. 14,15-Dihydroxyeicosatrienoic acid activates peroxisome proliferator-activated receptor-alpha. Am J Physiol Heart Circ Physiol. 2006; 290(1):H55–63. Epub 2005/08/23. https://doi.org/10.1152/ajpheart.00427.2005 PMID: 16113065.

33. Spector AA. Arachidonic acid cytochrome P450 epoxygenase pathway. J Lipid Res. 2009; 50 Suppl: S52–6. Epub 2008/10/28. https://doi.org/10.1194/jlr.R800038-JLR200 PMID: 18952572.

34. Spector AA, Norris AW. Action of epoxyeicosatrienoic acids on cellular function. Am J Physiol Cell Physiol. 2007; 292(3):C996–1012. Epub 2006/09/22. https://doi.org/10.1152/ajpcell.00402.2006 PMID: 16987999.

35. Zha W, Edin ML, Vendrov KC, Schuck RN, Lih FB, Jat JL, et al. Functional characterization of cytochrome P450-derived epoxyeicosatrienoic acids in adipogenesis and obesity. J Lipid Res. 2014; 55 (10):2124–36. https://doi.org/10.1194/jlr.M053199 PMID: 25114171;

36. Kim DH, Vanella L, Inoue K, Burgess A, Gotlinger K, Manthati VL, et al. Epoxyeicosatrienoic acid agonist regulates human mesenchymal stem cell-derived adipocytes through activation of HO-1-pAKT signaling and a decrease in PPARgamma. Stem cells and development. 2010; 19(12):1863–73. https://doi.org/10.1089/scd.2010.0098 PMID: 20412023;

37. Waldman M, Bellner L, Vanella L, Schragenheim J, Sodhi K, Singh SP, et al. Epoxyeicosatrienoic Acids Regulate Adipocyte Differentiation of Mouse 3T3 Cells, Via PGC-1alpha Activation, Which Is Required for HO-1 Expression and Increased Mitochondrial Function. Stem cells and development. 2016; 25 (14):1084–94. https://doi.org/10.1089/scd.2016.0072 PMID: 27224420;

38. El Hajj N, Pliushch G, Schneider E, Dittrich M, Muller T, Korenkov M, et al. Metabolic programming of MEST DNA methylation by intrauterine exposure to gestational diabetes mellitus. Diabetes. 2013; 62 (4):1320–8. https://doi.org/10.2337/db12-0289 PMID: 23209187;

39. Soubry A, Murphy SK, Wang F, Huang Z, Vidal AC, Fuemmeler BF, et al. Newborns of obese parents have altered DNA methylation patterns at imprinted genes. International journal of obesity. 2015; 39 (4):650–7. https://doi.org/10.1038/ijo.2013.193 PMID: 24158121;

40. Barbagallo I, Vanella L, Cambria MT, Tibullo D, Godos J, Guarnaccia L, et al. Silibinin Regulates Lipid Metabolism and Differentiation in Functional Human Adipocytes. Frontiers in pharmacology. 2015; 6:309. https://doi.org/10.3389/fphar.2015.00309 PMID: 26834634;

41. Karbiener M, Glantschnig C, Pisani DF, Laurencikiene J, Dahlman I, Herzig S, et al. Mesoderm-specific transcript (MEST) is a negative regulator of human adipocyte differentiation. International journal of obesity. 2015; 39(12):1733–41. https://doi.org/10.1038/ijo.2015.121 PMID: 26119994;

42. Kanwar YS, Kumar A, Ota K, Lin S, Wada J, Chugh S, et al. Identification of developmentally regulated mesodermal-specific transcript in mouse embryonic metanephros. Am J Physiol Renal Physiol. 2002; 282(5):F953–65. PMID: 11934706. https://doi.org/10.1152/ajprenal.00200.2001

43. Lefebvre L, Viville S, Barton SC, Ishino F, Keverne EB, Surani MA. Abnormal maternal behaviour and growth retardation associated with loss of the imprinted gene Mest. Nature genetics. 1998; 20(2):163–9. PMID: 9771709. https://doi.org/10.1038/2464

44. Lefebvre L, Viville S, Barton SC, Ishino F, Surani MA. Genomic structure and parent-of-origin-specific methylation of Peg1. Human molecular genetics. 1997; 6(11):1907–15. PMID: 9302270.

45. Tada M, Tada T, Lefebvre L, Barton SC, Surani MA. Embryonic germ cells induce epigenetic reprogramming of somatic nucleus in hybrid cells. The EMBO journal. 1997; 16(21):6510–20. PMID: 9351832. https://doi.org/10.1093/emboj/16.21.6510

46. Kamei Y, Suganami T, Kohda T, Ishino F, Yasuda K, Miura S, et al. Peg1/Mest in obese adipose tissue is expressed from the paternal allele in an isoform-specific manner. FEBS letters. 2007; 581(1):91–6. Epub 2006/12/22. https://doi.org/10.1016/j.febslet.2006.12.002 PMID: 17182038.

47. Nakanishi N, Nakagawa Y, Tokushige N, Aoki N, Matsuzaka T, Ishii K, et al. The up-regulation of microRNA-335 is associated with lipid metabolism in liver and white adipose tissue of genetically obese mice. Biochemical and biophysical research communications. 2009; 385(4):492–6. https://doi.org/10.1016/j.bbrc.2009.05.058 PMID: 19460359.

48. Zhu L, Chen L, Shi CM, Xu GF, Xu LL, Zhu LL, et al. MiR-335, an adipogenesis-related microRNA, is involved in adipose tissue inflammation. Cell biochemistry and biophysics. 2014; 68(2):283–90. https://doi.org/10.1007/s12013-013-9708-3 PMID: 23801157.

49. Dorn C, Riener MO, Kirovski G, Saugspier M, Steib K, Weiss TS, et al. Expression of fatty acid synthase in nonalcoholic fatty liver disease. International journal of clinical and experimental pathology. 2010; 3 (5):505–14. PMID: 20606731;

50. Kotronen A, Seppanen-Laakso T, Westerbacka J, Kiviluoto T, Arola J, Ruskeepaa AL, et al. Hepatic stearoyl-CoA desaturase (SCD)-1 activity and diacylglycerol but not ceramide concentrations are increased in the nonalcoholic human fatty liver. Diabetes. 2009; 58(1):203–8. https://doi.org/10.2337/db08-1074 PMID: 18952834;

51. Miyazaki M, Dobrzyn A, Sampath H, Lee SH, Man WC, Chu K, et al. Reduced adiposity and liver steatosis by stearoyl-CoA desaturase deficiency are independent of peroxisome proliferator-activated receptor-alpha. J Biol Chem. 2004; 279(33):35017–24. https://doi.org/10.1074/jbc.M405327200 PMID: 15180999.

52. Villanueva CJ, Monetti M, Shih M, Zhou P, Watkins SM, Bhanot S, et al. Specific role for acyl CoA:Diacylglycerol acyltransferase 1 (Dgat1) in hepatic steatosis due to exogenous fatty acids. Hepatology. 2009; 50(2):434–42. https://doi.org/10.1002/hep.22980 PMID: 19472314;

53. Christodoulides C, Lagathu C, Sethi JK, Vidal-Puig A. Adipogenesis and WNT signalling. Trends in endocrinology and metabolism: TEM. 2009; 20(1):16–24. https://doi.org/10.1016/j.tem.2008.09.002 PMID: 19008118;

54. Fuster JJ, Zuriaga MA, Ngo DT, Farb MG, Aprahamian T, Yamaguchi TP, et al. Noncanonical Wnt signaling promotes obesity-induced adipose tissue inflammation and metabolic dysfunction independent of adipose tissue expansion. Diabetes. 2015; 64(4):1235–48. https://doi.org/10.2337/db14-1164 PMID: 25352637;

55. Ross SE, Hemati N, Longo KA, Bennett CN, Lucas PC, Erickson RL, et al. Inhibition of adipogenesis by Wnt signaling. Science. 2000; 289(5481):950–3. PMID: 10937998.

56. Jablonski KA, Amici SA, Webb LM, Ruiz-Rosado Jde D, Popovich PG, Partida-Sanchez S, et al. Novel Markers to Delineate Murine M1 and M2 Macrophages. PLoS One. 2015; 10(12):e0145342. https://doi.org/10.1371/journal.pone.0145342 PMID: 26699615;

57. Rim JS, Mynatt RL, Gawronska-Kozak B. Mesenchymal stem cells from the outer ear: a novel adult stem cell model system for the study of adipogenesis. FASEB journal: official publication of the Federation of American Societies for Experimental Biology. 2005; 19(9):1205–7. PMID: 15857881. https://doi.org/10.1096/fj.04-3204fje

58. Chen YQ, Kuo MS, Li S, Bui HH, Peake DA, Sanders PE, et al. AGPAT6 is a novel microsomal glycerol-3-phosphate acyltransferase. J Biol Chem. 2008; 283(15):10048–57. https://doi.org/10.1074/jbc.M708151200 PMID: 18238778;

59. Beigneux AP, Vergnes L, Qiao X, Quatela S, Davis R, Watkins SM, et al. Agpat6—a novel lipid biosynthetic gene required for triacylglycerol production in mammary epithelium. J Lipid Res. 2006; 47 (4):734–44. https://doi.org/10.1194/jlr.M500556-JLR200 PMID: 16449762;

60. Jura M, Jaroslawska J, Chu DT, Kozak LP. Mest and Sfrp5 are biomarkers for healthy adipose tissue. Biochimie. 2016; 124:124–33. https://doi.org/10.1016/j.biochi.2015.05.006 PMID: 26001362.

61. Kumar RA, Chan KL, Wong AH, Little KQ, Rajcan-Separovic E, Abrahams BS, et al. Unexpected embryonic stem (ES) cell mutations represent a concern in gene targeting: lessons from "fierce" mice. Genesis. 2004; 38(2):51–7. https://doi.org/10.1002/gene.20001 PMID: 14994267.

62. Ineson J, Stayner C, Hazlett J, Slobbe L, Robson E, Legge M, et al. Somatic reactivation of expression of the silent maternal Mest allele and acquisition of normal reproductive behaviour in a colony of Peg1/Mest mutant mice. The Journal of reproduction and development. 2012; 58(4):490–500. PMID: 22522229.

63. Lin X, Wu L, Zhang Z, Yang R, Guan Q, Hou X, et al. MiR-335-5p promotes chondrogenesis in mouse mesenchymal stem cells and is regulated through two positive feedback loops. Journal of bone and mineral research: the official journal of the American Society for Bone and Mineral Research. 2014; 29 (7):1575–85. https://doi.org/10.1002/jbmr.2163 PMID: 24347469.

64. Hiramuki Y, Sato T, Furuta Y, Surani MA, Sehara-Fujisawa A. Mest but Not MiR-335 Affects Skeletal Muscle Growth and Regeneration. PLoS One. 2015; 10(6):e0130436. https://doi.org/10.1371/journal.pone.0130436 PMID: 26098312;

65. Anunciado-Koza RP, Higgins DC, Koza RA. Adipose tissue Mest and Sfrp5 are concomitant with variations of adiposity among inbred mouse strains fed a non-obesogenic diet. Biochimie. 2016; 124:134–40. https://doi.org/10.1016/j.biochi.2015.05.007 PMID: 26005096;

66. Asterholm IW, Halberg N, Scherer PE. Mouse Models of Lipodystrophy Key reagents for the understanding of the metabolic syndrome. Drug discovery today Disease models. 2007; 4(1):17–24. https://doi.org/10.1016/j.ddmod.2007.10.003 PMID: 18193096;

67. Huang-Doran I, Sleigh A, Rochford JJ, O'Rahilly S, Savage DB. Lipodystrophy: metabolic insights from a rare disorder. The Journal of endocrinology. 2010; 207(3):245–55. https://doi.org/10.1677/JOE-10-0272 PMID: 20870709.

68. Park SY, Choi GH, Choi HI, Ryu J, Jung CY, Lee W. Calorie restriction improves whole-body glucose disposal and insulin resistance in association with the increased adipocyte-specific GLUT4 expression in Otsuka Long-Evans Tokushima fatty rats. Archives of biochemistry and biophysics. 2005; 436 (2):276–84. https://doi.org/10.1016/j.abb.2005.01.010 PMID: 15797240.

69. Pires RC, Souza EE, Vanzela EC, Ribeiro RA, Silva-Santos JC, Carneiro EM, et al. Short-term calorie restriction improves glucose homeostasis in old rats: involvement of AMPK. Applied physiology, nutrition, and metabolism = Physiologie appliquee, nutrition et metabolisme. 2014; 39(8):895–901. https://doi.org/10.1139/apnm-2013-0520 PMID: 24844367.

70. Rosen ED, Spiegelman BM. Adipocytes as regulators of energy balance and glucose homeostasis. Nature. 2006; 444(7121):847–53. https://doi.org/10.1038/nature05483 PMID: 17167472;

71. Stanford KI, Middelbeek RJ, Townsend KL, An D, Nygaard EB, Hitchcox KM, et al. Brown adipose tissue regulates glucose homeostasis and insulin sensitivity. The Journal of clinical investigation. 2013; 123(1):215–23. https://doi.org/10.1172/JCI62308 PMID: 23221344;

72. Weiss EP, Racette SB, Villareal DT, Fontana L, Steger-May K, Schechtman KB, et al. Improvements in glucose tolerance and insulin action induced by increasing energy expenditure or decreasing energy intake: a randomized controlled trial. The American journal of clinical nutrition. 2006; 84(5):1033–42. PMID: 17093155;

73. Zietak M, Kovatcheva-Datchary P, Markiewicz LH, Stahlman M, Kozak LP, Backhed F. Altered Microbiota Contributes to Reduced Diet-Induced Obesity upon Cold Exposure. Cell metabolism. 2016; 23 (6):1216–23. https://doi.org/10.1016/j.cmet.2016.05.001 PMID: 27304513;

74. Wilfling F, Wang H, Haas JT, Krahmer N, Gould TJ, Uchida A, et al. Triacylglycerol synthesis enzymes mediate lipid droplet growth by relocalizing from the ER to lipid droplets. Developmental cell. 2013; 24 (4):384–99. https://doi.org/10.1016/j.devcel.2013.01.013 PMID: 23415954;

75. Cheng XY, Huang WJ, Hu SC, Zhang HL, Wang H, Zhang JX, et al. A global characterization and identification of multifunctional enzymes. PLoS One. 2012; 7(6):e38979. https://doi.org/10.1371/journal.pone.0038979 PMID: 22723914;

76. Lenfant N, Hotelier T, Velluet E, Bourne Y, Marchot P, Chatonnet A. ESTHER, the database of the alpha/beta-hydrolase fold superfamily of proteins: tools to explore diversity of functions. Nucleic acids research. 2013; 41(Database issue):D423–9. https://doi.org/10.1093/nar/gks1154 PMID: 23193256;

77. Marchot P, Chatonnet A. Enzymatic activity and protein interactions in alpha/beta hydrolase fold proteins: moonlighting versus promiscuity. Protein and peptide letters. 2012; 19(2):132–43. PMID: 21933125.

78. Vergnes L, Beigneux AP, Davis R, Watkins SM, Young SG, Reue K. Agpat6 deficiency causes subdermal lipodystrophy and resistance to obesity. J Lipid Res. 2006; 47(4):745–54. https://doi.org/10.1194/jlr.M500553-JLR200 PMID: 16436371;

79. Lakso M, Pichel JG, Gorman JR, Sauer B, Okamoto Y, Lee E, et al. Efficient in vivo manipulation of mouse genomic sequences at the zygote stage. Proc Natl Acad Sci U S A. 1996; 93(12):5860–5. PMID: 8650183;

80. Zemany L, Kraus BJ, Norseen J, Saito T, Peroni OD, Johnson RL, et al. Downregulation of STRA6 in adipocytes and adipose stromovascular fraction in obesity and effects of adipocyte-specific STRA6 knockdown in vivo. Molecular and cellular biology. 2014; 34(6):1170–86. https://doi.org/10.1128/MCB.01106-13 PMID: 24421389;

81. Tibshirani R, Hastie T, Narasimhan B, Chu G. Diagnosis of multiple cancer types by shrunken centroids of gene expression. Proc Natl Acad Sci U S A. 2002; 99(10):6567–72. https://doi.org/10.1073/pnas.082099299 PMID: 12011421;

82. Tusher VG, Tibshirani R, Chu G. Significance analysis of microarrays applied to the ionizing radiation response. Proc Natl Acad Sci U S A. 2001; 98(9):5116–21. https://doi.org/10.1073/pnas.091062498 PMID: 11309499;

83. Benjamini Y, Hochberg Y. Controlling the false discovery rate: A practical and powerful approach to multiple testing. J R Stat Soc B. 1995; 57(1):289–300.